THESIS

COMPUTER AIDED ENGINEERING OF AN AUTOMOBILE GASOLINE REFUELING SYSTEM

Submitted by

Mangesh Dake

Department of Mechanical Engineering

In partial fulfillment of the requirements

For the Degree of Master of Science

Colorado State University

Fort Collins, Colorado

Fall 2018

Master's Committee:

Advisor: Bret C. Windom

Anthony J. Marchese
Karan S. Venayagamoorthy

ABSTRACT

COMPUTER AIDED ENGINEERING OF AN AUTOMOBILE GASOLINE REFUELING SYSTEM

A vehicle's refueling system, including components which make up the Onboard Refueling Vapor Recovery (ORVR) system, must be designed to meet federally set evaporative hydrocarbon emission regulations and other performance issues inherent to the refueling process, such as premature click-off of the refueling nozzle and spit-back. A Computational Fluid Dynamics (CFD) model able to predict the performance of a vehicle's refueling system could be a valuable tool towards the development of future gasoline refueling system designs, saving the Original Equipment Manufacturer's time and money currently invested in the research and development of these systems. To create an adequate model required for Computer Aided Engineering (CAE) of a modern refueling system, it is paramount to accurately predict the fluid dynamics through and out of a gasoline refueling nozzle, within the different components inside the refueling system, and the outlets of the fuel tank. Using CFD, this study aims to predict the performance of a refueling system. The commercial CFD software, Star-CCM+, was used to model fuel flow through a currently in production refueling system geometry. Experiments were conducted using a test setup to mimic the simulated refueling system to carefully describe the system's boundary and initial conditions and to evaluate the CFD results. It was found that modeling of the fluid dynamics through the air entrainment and pressure port geometries within the refueling nozzle were needed to accurately capture fuel spray behavior as demonstrated by experiments. By monitoring the amount of liquid fuel contacting the pressure port on the refueling nozzle, the simulations are able

to identify fillerpipe designs that fail as a result of early click-off. Simulations of the complete refueling system, while neglecting phase change of the fuel, were able to predict the trends and dynamics of the tank pressure experienced by the experiments for varying fuel pump flow rates. The study acts as a guide for future refueling simulations involving fuel evaporation, for which initial results are presented.

ACKNOWLEDGMENTS

I extend my gratitude to my academic advisor Dr. Bret Windom for his inspiration, timely guidance and financial support throughout my studies at Colorado State University. I am very glad to be part of his research team, which helped me gain valuable experience of latest industrial problems.

I am thankful to my exam committee Dr. Anthony Marchese and Dr. Karan Venayagamoorthy for their guidance and thoughtful suggestions.

I would like to thank Honda R&D engineers Marc Henderson, Joshua Shaw, Matthew Swanson and Randy Fabrizio for their insight and expertise, which has contributed greatly to the progress of this thesis. Thanks to Steve Walters and Steve Capaldi for their help with importing surface repaired geometries.

I would also like to thank all members from senior design team and graduate student McKay Stoker who worked hard on the experimental side of the project. A special thank goes to Luke Nibblelink and Joe FitzWilliam who went beyond their duties to help me with the experiment setup.

TABLE OF CONTENTS

1 Introduction

Historically, during the refueling process of a gasoline fueled vehicle, environmentally harmful hydrocarbon (gasoline) vapors were vented into the atmosphere as the liquid fuel displaced the fuel vapor (residing in the headspace of the empty tank). The Environmental Protection Agency (EPA) has been regulating hydrocarbon vapor emissions in the United States since the 1970s when it was decided that Stage II control systems were necessary for all areas of non-attainment (or areas where the National Ambient Air Quality Standards were not met). Following the Clean Air Act of 1990, the Stage II vapor recovery systems became mandatory and were installed on fuel dispensing stations throughout the United States. Stage II recovery systems manifested themselves in the form of rubber vapor covers on gasoline nozzles at refueling stations which would siphon the volatile organic compounds (VOC's) emitted from the vehicle during the refueling process into the fueling station's underground gasoline storage tank[1]. However, after 2012, the Stage II systems were deregulated by the EPA due to the high cost and poor performance[2]. In replace of the Stage II systems, the EPA implemented regulations on the automotive OEMs to design and install more effective vapor recovery systems which would retain all fuel vapor on the vehicle during the refueling process. These devices are known as Onboard Refueling Vapor Recovery (ORVR) systems. ORVR systems are approximately 98% efficient as per EPA estimate. Additionally, they are very reliable and cost effective because of the value of the fuel being conserved. ORVR systems are standard on all consumer cars post model year 2000 and all consumer trucks post model year 2007[3]. ORVR systems are efficient at capturing refueling vapors with no degradation over time, compared to steady degradation of Stage II systems[1].

The main component of the system is the activated carbon canister, which absorbs the hydrocarbons generated in fuel tank. These hydrocarbons are then purged from the canister and sent to engine for combustion[4]. This device costs approximately $100 to the OEM. Using this device helps to reduce the evaporation loss of the fuel. This subsequently causes less VOCs and increase in fuel economy (by combusting the fuel in engine instead of evaporation). The average US vehicle generates ~30 g HC/day of evaporative emissions without ORVR system. There are approximately 200,000,000 vehicles in US. Therefore, the amount of fuel that can evaporate in atmosphere will be 6,000,000 kg/day (or in other words 2,127,792 gallon of fuel loss/day). If an ORVR system is installed the fuel can be used in the engine. US fuel consumption is 390,000,000 gallon/day. That means after installing ORVR system the vehicle is saving 0.5% fuel[5].

A general schematic of a typical ORVR system is demonstrated in Figure 1.1, illustrating the major components and the fluid flow which occur during refueling. These systems work by redirecting the gasoline vapor displaced during refueling into an activated charcoal filled collection canister which absorbs the fuel vapors. The vapor displaced from the fuel tank may also travel through the vapor return line which consists of a pipe and a check valve. Vapor return line connects the tank and inlet of fuel filler neck and is used to limit entrained air while allowing the vapor to be re-dissolved back into the incoming liquid fuel stream. After refueling is finished, the hydrocarbons from the activated charcoal canister are purged into the engine intake system and combusted during normal engine operation.

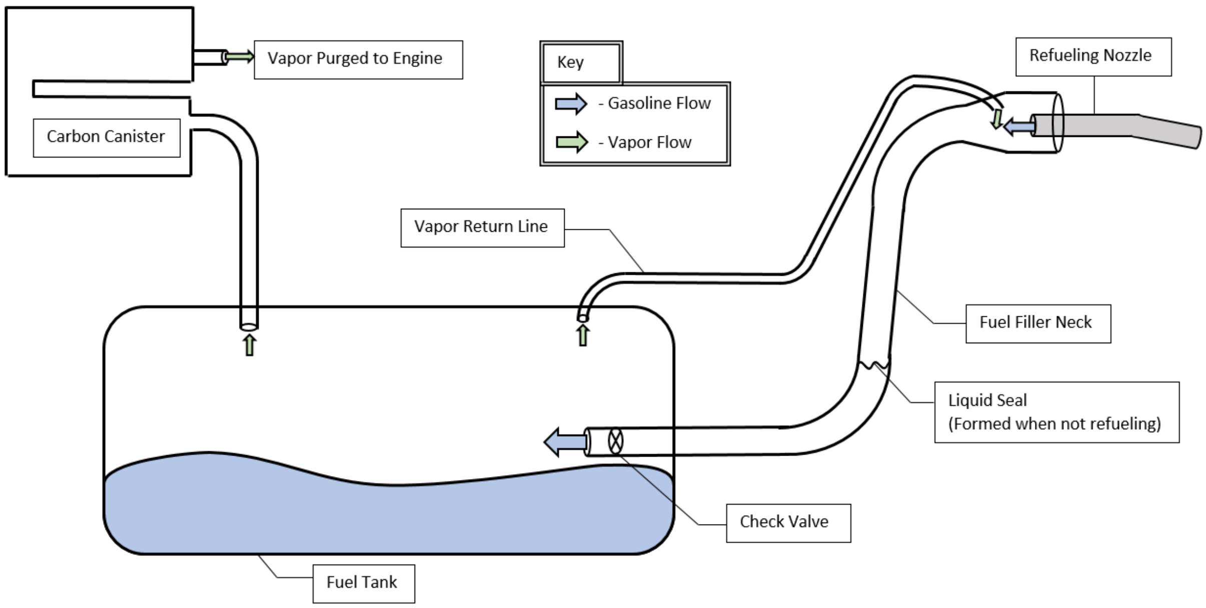

Figure 1.1 Simple schematic of a typical ORVR System

In order to be sold as road-going vehicles in the United States, motor vehicles need to pass EPA regulations for the maximum allowable amount of hydrocarbon vapor emissions during refueling (via escaping vapor or fuel spit-back)[6]. Currently the maximum amount of VOC's which can escape the fuel system is 0.2 grams per gallon of pumped gasoline. Automotive OEMs must abide by the EPA regulations for vapor emission when designing refueling/ORVR systems. Very briefly, the standardized test procedure measures total hydrocarbon vapor mass during the refueling by carrying out the measurement under a Sealed Housing for Evaporative Emission Determination (SHED). Prior to the measurement, the fuel tank is pre-filled (2.4 gal) and allowed to soak for 6 to 24 hours at 80 °F. During the measurement, the incoming fuel is kept at 67 °F and supplied at a dispensing rate of 9.8±0.3 gal/min. While refueling, data is recorded until the tank is filled to 95% of its capacity. Tests are repeated at additional dispensing rates between 4.0 and 9.8 gal/min[7].

In addition to designing to meet EPA vapor emission requirements, OEMs often have internal objectives for the design of the refueling system that are related to the system performance stemming from customer satisfaction. The primary performance criteria, which must be met are as follows:

(1) The tank must reach certain capacity without premature click-off. Premature click-off is premature triggering of the shut off mechanism in the nozzle.

(2) No occurrence of fuel spit-back (the ejection of liquid fuel out of the vehicle onto or around the customer). Fuel spit-back can result from rapid tank depressurization when the filler pipe is opened to ambient conditions. A reverse vapor flow leading to spit-back can be created if the fuel tank or filler pipe pressure level is too high, thus making the fuel tank pressure an important consideration. Spit back will also guarantee a failed ORVR test result[8].

Current design practices for the refueling system require prototyping and testing of the fuel system to ensure that it meets EPA requirements and performance criteria set forth by the manufacturer. During the course of designing a vehicle, the fuel system requires several design iterations. For each new design, the system must be tested again. This iterative design-build process can require substantial engineer and production time resulting in a very expensive process. To assist the design of a refueling system, a validated Computer Aided Engineering (CAE) model is being developed which will complement and possibly supplant the existing iterative refueling system design process. The following chapters describes the state of the art of CAE modeling for multi-phase flowing systems and validation techniques which will be leveraged during the development and testing of a refueling system CAE model.

1.1 Thesis Organization

In the following chapters, the literature review, system description, simulation setup and results from simulation that evaluate performance of refueling system are discussed in detail.

Chapter 2 presents a literature review of experimental and computational efforts aimed at understanding and characterizing refueling systems. Three previous theses which have attempted to characterize a refueling system using mathematical code/commercial software are discussed first. Followed by relevant research papers on the modeling of refueling nozzles and 2D simulation of refueling systems are also discussed.

Chapter 3 describes the CFD setup including Volume Of Fluid (VOF) modeling which is used to track the free surface of the fuel in all simulations of this study along with details of the meshing strategy and CFD parameters used throughout.

Chapter 4 and 5 provides in detail the characterization of the system boundaries and the geometry manipulations performed to setup the CFD domain. Details of the refueling nozzle are given, which was found to be an important boundary. The methods applied to characterize the boundaries used in the simulations are discussed in detail in this chapter.

This study has been divided into two parts. Chapter 6 explains Part – 1 of the study where only the fillerpipe and nozzle is considered. Experiments are carried out isolated to an open system with only fuel flowing through the nozzle and fillerpipe and then to a bucket. Two fillerpipes are tested and their tendency to lead to early click-off evaluated.

Chapter 7 explains Part – II of the study. In Part – II, all the components of a refueling system are considered, including the tank and all inlet and outlet boundaries connected to it. Experiments are carried out at different fuel dispensing rates. Pressure in the tank and flow rate is recorded. Simulations are carried out as per experimental conditions and the simulation results are compared against the experiments.

Chapter 8 summarizes the outcomes of the study and gives some ideas about future work of this study.

2 Literature Review

2.1 Background

There are numerous examples from literature that are relevant to the work to be carried out in this project. Published journal articles, academic theses, and the CAE technical literature have been reviewed and serve as the sources for the following background study. Modeling of a gasoline refueling system presents many challenges including the need to account for physics related to multi-phase fluid dynamics, phase change, turbulence and heat transfer for irregular geometries. These challenges encountered by previous studies are also highlighted. Because of the complexity of this problem, there is a need for experimental validation to determine the relative importance, accuracy, and limitations of the multiple physical models available in commercially available CAE platforms over a wide range of operating conditions. As this experimental design and research phase is paramount for the successful completion of the project, related research focused on the experimental measurements of phenomenon deemed relevant to the dynamics of the refueling system have also been reviewed.

2.2 Previous Work and Results

A master's thesis by Maurizio Mastroianni from the University of Windsor in 2000, details an experimental study investigating the fluid dynamics encountered in a refueling system. The author uses a fuel conditioning cart, controlling fuel flow rates and temperature, to flow gasoline through a simple filler neck into a rectangular tank, which includes a vapor return line. Temperature and pressure measurements were made at multiple points along the filler neck and fuel tank. Filling performance, such as fuel build-up which leads to early click-off and spit-back, was the focus of this paper, and higher flow-rates (10 & 12 GPM) and Reid Vapor Pressure (RVP

– 83 and 55 kPa) blends of gasoline were tested. Dimensional analysis was used to determine influential variables for filling performance in relation to spit back and early click-off. It was found that the vapor return line diameter is a critical parameter of the fuel system. Note that the canister is not part of experimental setup. For all tests, smaller diameter vent tubes (vapor return line is called vent tube in Mastroianni's study) caused early click-off while larger diameter vent tubes allowed for little fuel buildup. Increase in fuel RVP and flow rates increases the highest pressure recorded but did not always lead to early click-off[9].

A master's thesis by Kristoffer Johansson at the Chalmers University of Technology in Sweden from 2011 detailed work sponsored by Volvo leading to the development of a CAE model of a refueling system. Using gasoline as the fuel of interest, this study developed and tested a CAE model in ANSYS FLUENT. The original objective of the work was to check if the fuel tank could be replaced with a pressure resistance in the CAE model. Generally, the volume of the fillerpipe is around 2 liters and the volume of the fuel tank is more than 70 liters. Therefore, the mesh in the tank is significantly big as compared to fillerneck. Neglecting tank will reduce the computational time by a huge margin. However, the visualization validation experiments failed due to the incompatibility between the piping material and the gasoline. The paper only simulates the filler pipe flow, without the fuel tank or vapor return, similar to part – 1 of the present work. For the simulations, time step was in range of microseconds and cell count was in range of 3 million. Generally, for different combinations of mesh type and time step created by Johansson required 2 weeks for a single simulation. Due to lack of time, only few combinations were tested. Experimental validation was lacking leaving questions about the recommendations regarding the meshing strategies. Furthermore, with experimental validation it was not confirmed whether the tank needs to be present during the simulation or not[10].

A master's thesis by Michael Gunnesby at the Linköpings University from 2015 also sponsored by the Volvo Car Corporation (VCC) described in great detail a CAE model that was developed to predict fuel (diesel) flow in the filler pipe. The primary focus of the work was related to the problem of early click-off. As diesel fuel has a much lower vapor pressure than gasoline, vapor generation was of little concern and early click-off was considered the worst-case scenario of the refueling process. The flow of diesel fuel was tested and modeled at high volumetric flow rates of 55 l/min (14.5 GPM) to match closely with commercial fuel dispensing flow rates. This value is higher than typical gasoline flow rates which are often around 10 GPM. Due to limitations of computational resources the simulations were only focused on the first second of the refueling process, as it was determined via experiments that early click-off with these high flow rates was most likely to occur within the first few seconds following fuel addition. The CAE model was developed using Star-CCM+, the same software to be used in this project, and provides valuable information on the model development including grid independence and mesh/time-step size that can serve as a starting point for the present work[11].

Gunnesby also carried out experiments to validate their developed models. The experiments obtained pressure data from a series of pressure transducers in a transparent tubing on both a simplified and full (production) filler neck geometries, which were produced via 3D-printing acrylic plastic pipe. Figure 2.1 depicts the experimental setup used in this work. The experiments were repeated several times and average values were calculated. Four point probes are set in the simulation geometry at identical locations of the pressure transducers, and static pressure at that particular location is tracked and plotted vs time and compared with the experimentally measured values. Accompanying the transient pressure data, high-speed video recording (480 fps) is also used to monitor the flow shape and phenomenon to compare with the simulation results. Multiple simulations were carried with different turbulent models including Unsteady Reynolds Averaged Navier Stokes (URANS), Large Eddy Simulation (LES), and Detached Eddy Simulation (DES). Figure 2.2 compares the pressure data at the entry of the filler neck collected from the simulations and the experiments.

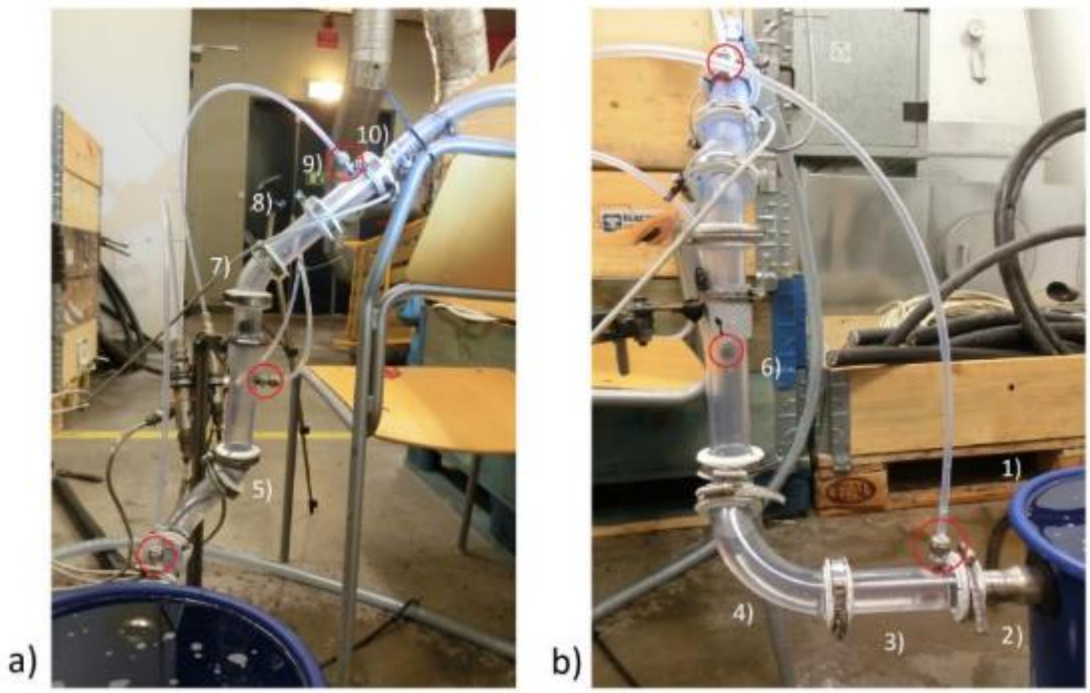

Figure 2.1 Experimental platform used by Gunnesby. Red circles represent location of pressure transducers

Clearly there are discrepancies between the models and the experiments during the initial startup. At later times, however, good agreement is noted between the experiments and the model utilizing the URANS, the SST k- ω turbulence model. The model predicted the occurrence of spit-back which was also observed in experiments. The red circles in Figure 4 mark the times associated with spit-back for both the model and experiments. Clearly, there is an inability to predict flow phenomenon during the initial startup of the flow. The poor agreement was attributed to the non-uniform temporal and spatial flow profile when the nozzle is actuated. Indeed, this can never be a precise condition since the opening of a valve to start flow is transient process often operated by hand, but with the help of high-speed video recording (480 fps), the opening of the valve was shown to transition from no flow to steady flow in 0.1 s for each experiment. To account for the transient start-up experienced in the experiments, the model utilized an inlet condition where the mass flow rate was defined by a field function as:

If $t \leq 0.1$

$\dot{m} = 93.1 \times t^2 (\frac{kg}{s})$

Else,

$\dot{m} = 0.931\ (\frac{kg}{s})$ Eq. 2.1

This inlet function exponentially ramps up mass flow until 0.1 seconds. The value 0.931 kg/s corresponds to 56 l/min of diesel fuel[11].

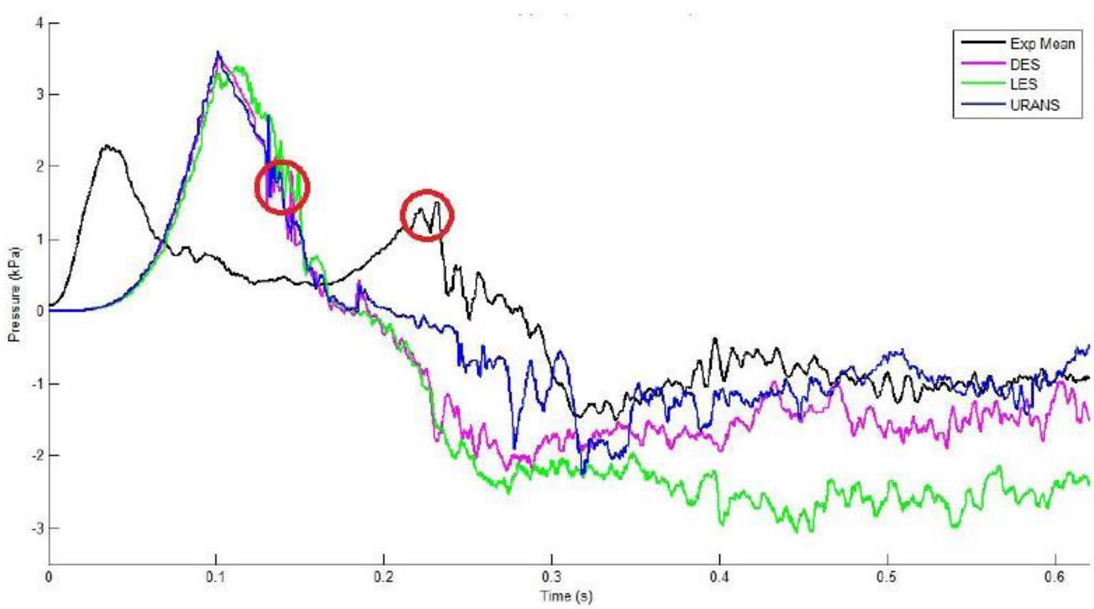

Figure 2.2 Results by Gunnesby demonstrating the pressure comparison at the filler inlet between CAE and experiments

The work by Gunnesby was focused on diesel refueling and thus did not consider vapor generation, however, others have investigated the role of phase change and two phase flow on the dynamics of a refueling system. Simulating multi-component multi-phase phenomenon is a formidable task. Because the two phases will be at different temperatures, which would lead to heat transfer between the two phases. Heat of vaporization would serve to further reduce the temperature of the liquid phase through evaporative cooling. Multicomponent mixtures would lead to multicomponent diffusion interactions leading to special mass transport phenomena, such as osmotic diffusion and reverse diffusion. Additionally, due to evaporation, there would be interphase mass transfer. The paper by Banerjee explored the feasibility of multiple assumptions when developing a CAE model of a gasoline refueling system. The model was simplified by treating the system as isothermal, neglecting buoyancy effects and thus only considering forced convection, and assuming composition independent gas phase properties. CAE simulations of two-phase multicomponent (gasoline and air) flow inside the fuel filler pipe with various flow rate were performed. A commercial CAE package, FLUENT 5.5 was used for the simulations[12]. Though no experimental comparison was made to the model predictions, interesting trends relating fuel dispensing rates and hydrocarbon vapor emissions were noticed.

In a study by Hassanvand et. al., evaporation was evaluated during the splash loading of a two-dimensional fuel tank with help of a 2D mesh in a commercial CFD software. It was observed that during submerged loading (when the outlet of filler pipe is at the bottom of the tank) liquid turbulence is controlled significantly, resulting in much lower vapor emission than encountered during splash (top) loading. The authors also showed that evaporative emissions depend upon fuel volatility, vehicle fuel system design, and driving conditions such as temperature variation, parking time, trip length, etc. This paper did not show any experimental validation, but does give a good idea about which factors affect fuel evaporation. For example, as seen in Figure 2.3, by using a 2D model, it is found that by increasing the inlet flow velocity of fuel, the rate of evaporation increases. However, at a higher velocity, the fuel tank fills in less time and can lead to a decrease in total evaporated mass. In addition, temperature has a huge impact on vapor emissions: as an example, a 6% change in temperature was shown to cause a 300 – 500% increase in vapor emissions[13]. An empirical relation is given in the paper to calculate vapor emissions during splash loading of fuel tank:

$$L_L = 202\, Re^{-0.42} (\frac{P_{vap}}{T})^{0.92} 0.293^{S} \qquad \text{Eq. 2.2}$$

Where L_L is the loading loss (lb/10^3 gal), S is an empirical saturation factor, P_{vap} is the vapor pressure of loaded liquid (psia), T is temperature of bulk liquid and Re is Reynolds number[13].

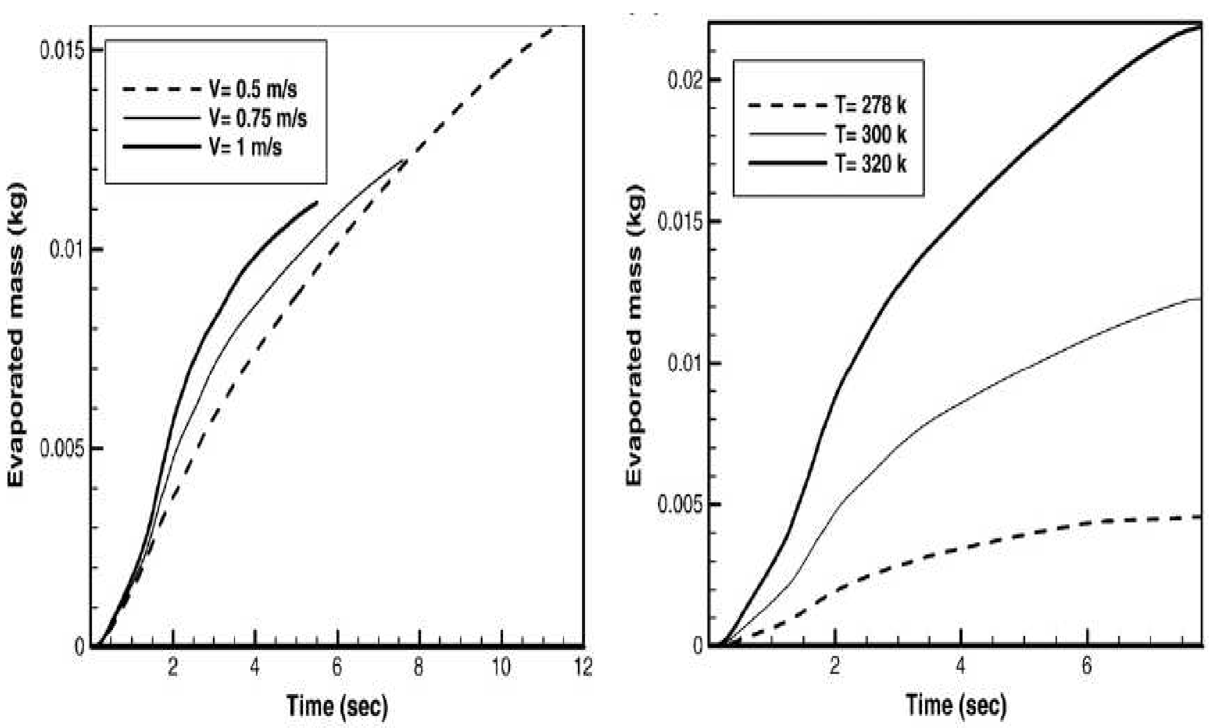

Figure 2.3 Effect of inlet velocity and temperature on gasoline evaporation during fuel tank loading

In another study by Banerjee and Isaac, CAE modeling coupled with complementary experimental validation of an automotive filler pipe was successfully carried out and provided additional understanding on how to treat the complex two-phase flow. Low flow rates were tested and dyes were used to see features of swirl and air entrainment. Surface roughness values were accurately measured and used in CAE simulations. To select the appropriate turbulence model, air entrainment values were compared. The time step used for this simulation was 0.0001sec. Many interesting features of the flow were uncovered, such as laminar-to-turbulent transition, progressive development of strong swirl along filler pipe axis, air entrainment, and mixing with the liquid were observed in the experiments leading to a better understanding of the processes of practical importance such as air entrainment and vapor emissions. The rate of air entrainment was shown to increase with increasing liquid fuel flow rates[12].

The fuel filling nozzle is also a major component of refueling system as this represents the primary boundary condition for the fuel inlet. There are many types of nozzles and their characteristics can vary. It is necessary to develop the boundary condition information for this component as well. Among those characteristics, air entrainment though the shut-off port into the dispensed fuel is of concern. As detailed in[14], air entrainment can be measured by installing a collar connected to a flow meter and a manometer over the shut-off sensor port on the nozzle. This measurement was adopted in the current study to select appropriate nozzle boundary conditions in the CAE simulations.

3 CFD Approach

3.1 Volume of Fluid (VOF) Mathematical Formulation

As observed in the experimental studies, the flow is highly turbulent and can be considered as stratified two phase flow with air and fluid as two different phases[8], [13]. Several multiphase models are available to simulate multi-phase flow such as Eulerian, Lagrangian, Dispersed, etc. However, multiphase modelling in this study was performed using the Volume of Fluid (VOF) model with the volume fraction condition required at the mass flow inlet derived from air entrainment measurements discussed later. VOF is well suited for this study and has been suggested by previous studies[11], [12].

The Volume of Fluid (VOF) multiphase model solves only one set of conservation equations, which is shared by multiple phases (and possibly multiple fluid types). VOF tracks the volume fraction of each phase throughout the domain. VOF modeling approach assumes that the mesh resolution is sufficient to resolve the position and the shape of the interface between the phases. In contrast, the Eulerian approach solves each phase separately and thus is significantly more computationally expensive. A Lagrangian approach considers fluid as small packets, not as a continuum, and is generally used for fluids like sand or gravel. Finally, the Dispersed multi-phase model is used in situations where fluid film formations on a solid surface are important[3].

The distribution of phases and the position of the interface are described by the fields of the phase volume fraction α_i. The volume fraction of phase i is defined as:

$$\alpha_i = \frac{V_i}{V} \qquad \text{Eq. 3.1}$$

Where V_i is the volume of phase *i* in the cell and V is the volume of the cell. In addition, the volume fractions of all phases in a cell must sum up to one:

$$\sum_{i=1}^{N} \alpha_i = 1 \qquad \text{Eq. 3.2}$$

Where *N* is the total number of phases. For this study, the number of phases are two. Depending on the value of the volume fraction, the presence of different phases or fluids in a cell can be distinguished. For $\alpha_i = 0$ the cell is completely void of phase i, for $\alpha_i = 1$ the cell is completely filled with phase i, and anything in between 1 and 0 represents interface between two phases. For practical purposes, it is widely accepted that a value of 0.3 be considered separated phases with a developing interface and 0.5 to be considered a fully developed separated interface[15]–[18].

The material properties that are calculated in the cells containing the interface depend on the material properties of the constituent fluids and their phase volume fraction of each species. The fluids that are present in the same interface-containing cell are treated as a mixture:

$$\rho = \sum_i \rho_i \alpha_i \qquad \text{Eq. 3.3}$$

$$\mu = \sum_i \mu_i \alpha_i \qquad \text{Eq. 3.4}$$

$$C_p = \sum_i \frac{(C_p)_i \rho_i}{\rho} \alpha_i \qquad \text{Eq. 3.5}$$

Where ρ_i is the density, μ_i is the dynamic viscosity, and $(C_p)_i$ is the specific heat of phase i. The distribution of a particular phase i is driven by the phase mass conservation equation:

$$\frac{\partial}{\partial t} \int_V \alpha_i \, dV + \oint_A \alpha_i \, v \cdot \mathrm{da} = \int_V \left(S_{\alpha_i} - \frac{\alpha_i}{\rho_i} \frac{D\rho_i}{Dt}\right) dV \qquad \text{Eq. 3.6}$$

Where a is the surface area vector, v is the velocity, S_{α_i} is a user-defined source term of phase i, and $D\rho_i/Dt$ is the material or Lagrangian derivative of the phase densities ρ_i.

In order to incorporate a phase change the source term can be a constant value, a user defined field function or by adding the Condensation- Evaporation model in STAR CCM+. For this study, phase change is not considered as it has very little effect on the spray pattern of the nozzle and incorporating evaporation physics results in significant additional compute time[19]–[22].

3.2 Courant Number

It can be difficult to converge to a solution when modeling multi-phase turbulent flow with phase change and heat and mass transfer. In addition, accounting for all the necessary physics can make the simulations highly computationally expensive. Meshing of the domain is a critical component in reducing computational time and generating reliable solutions. Computation time can be reduced by decreasing mesh size and/or increasing time steps but this occurs at the expense of accuracy. Guidelines to set mesh size and time step can be obtained from the Courant number:

$$\text{Courant Number} = \frac{u\,\Delta t}{\Delta x} \qquad \text{Eq. 3.7}$$

Where u is the magnitude of the velocity, Δt is the time step and Δx is the mesh size length interval. The value of the Courant number should always be less than 1. The Courant number is directly proportional to the time step and inversely proportional to mesh size. Since one must keep the Courant number within limits, any change in mesh must come with a change in time step[23].

Polyhedral cells with prism layers were found out to be very efficient for refueling systems in Gunnesby's study. Polyhedral cell have more cell faces than tetrahedral cells and thus allows for less numerical diffusion (when the simulated medium/fluid undergoes a higher diffusivity than the true medium). Whereas prism layers are used in order to increase the cell count near the wall to capture the gradients imposed by a surface.

The Reynolds numbers of the fuel exiting the refueling nozzle at a flow rate of 10 GPM is approximately 40000. In this section of the refueling system the fluid dynamics is considered to be highly turbulent. A K-Epsilon turbulence model was applied to model the fluid flow through refueling nozzle, into the filler pipe and finally into the tank [11].

4 System Description

In this chapter, the boundary conditions of refueling system are explained. The boundary conditions are the most critical component for a CFD model to properly predict the experiment. For both the CFD and the experiments, it is essential that the boundary conditions are correct and accurately described. Figure 4.1 shows a schematic of all the boundaries of a refueling system.

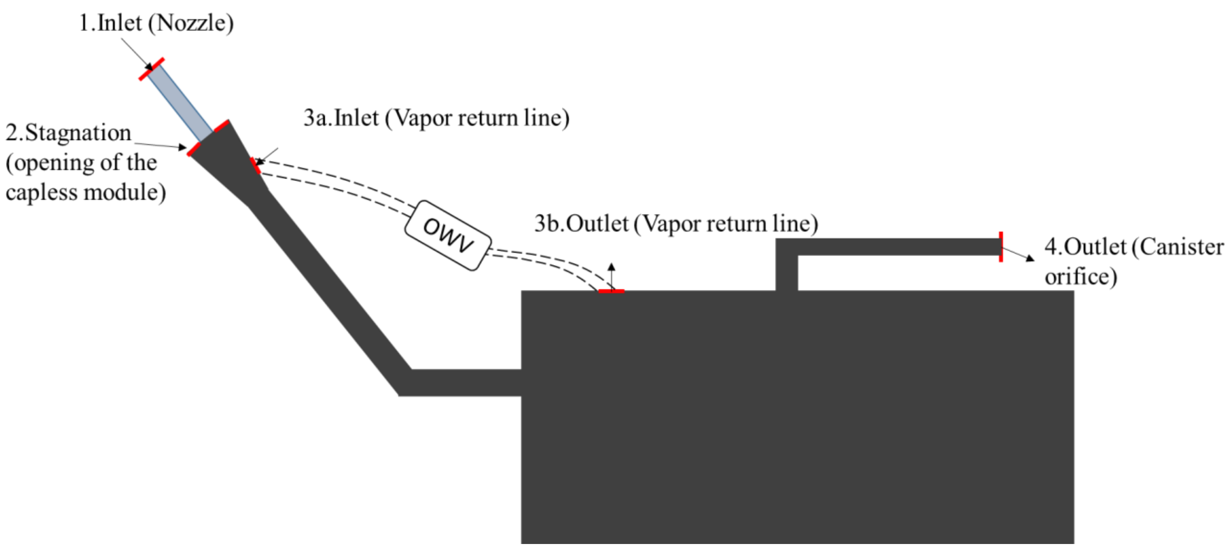

Figure 4.1 Boundary conditions of a refueling system

The vapor return line recirculates the saturated vapor from the tank to the opening of the fillerpipe near the refueling nozzle. Due to the complex geometry of the vapor return line (shown by dotted line in Figure 4.1), it has not been meshed and simulated, rather, two boundaries (3a and 3b) were used. The following sections will explain each of the boundary conditions in detail.

4.1 Boundary 1 – Refueling Nozzle

To create an adequate model for the computer aided engineering of a modern refueling system, it is paramount to accurately predict the fluid dynamics through and out of a gasoline refueling nozzle, as this is a key inlet condition of any refueling system. The fuel nozzle represents a critical boundary condition for modeling a refueling system and must be accurately defined. Furthermore, there are multiple nozzle types/designs with each having their own unique outlet fuel velocity and volume fraction pattern. Considerations related to accurately modeling this important boundary condition is presented in this section.

To date, previous work related to the CFD modelling of refueling systems have not considered the impact of nozzle geometry on the inlet condition and its subsequent impact on the CFD of the refueling system. To exclude associated uncertainties with using inappropriate boundary conditions due to inaccurate nozzle outlet flow, previous studies focused on modeling refueling systems, have replaced nozzle inlet conditions with a straight tube in both simulations and experimental validation [11]. It is critical that CFD predict the dynamics for inlet/boundary conditions that match OEM nozzle hardware. Similar work, though relatively limited, has explored the CFD modelling of a refueling nozzle. Banjaree et. al in 2007, using water as the test fluid for safety reasons, provided a detailed explanation regarding the interworking of a nozzle and proposed an experimental method to measure air entrainment flow rates. The work describes a method to measure spray patterns exiting from the nozzle, which was used to correlate the CFD. The paper also demonstrates the utilization of commercial CFD packages to successfully model nozzle spray patterns using multiphase Volume Of Fluid (VOF) physics and K- Epsilon turbulence model[12], [14], [24], [25].

Significant differences between the two nozzles when it comes to flow patterns are noted. Details regarding nozzle spray measurements, air entrainment measurements, geometry creation and manipulation are discussed. In addition, simulation details regarding mesh and time stepping strategies as well as the different techniques used to model air entrainment are described.

4.1.1 Experiment Description

4.1.1.1 Nozzle Spray Pattern measurement

To evaluate CFD results and the impact of modeling parameters (including geometrical influences and boundary conditions) on the fidelity of the model, it is necessary to compare to carefully collected data from a highly controlled experiment which is easy to execute, measure, reproduce, and simulate in a CFD domain. In this study, spray divergence measurements were carried out for two commercially available nozzles, an OPW 11B and a Husky X1, and used to validate predictions from a CFD simulation. In the experiments, the nozzles were oriented such that their outlets were at 45° with the horizontal, as seen in Figure 4.2. This was chosen since this orientation is similar to how a nozzle rests during refueling, and is simple to recreate in CFD. Images of the freely open fuel sprays were collected and analyzed to measure the width of the fuel spray perpendicular to the normal vector of the nozzle outlet at a location 250 mm downstream from the nozzle exit. A tape measure placed in the same plane as the nozzle and used to calibrate the image pixels into distance. Experiments were carried out at various flow rates in the range of 4 to 10 GPM (GPM). A fuel cart was used to deliver repeatable flow rates which were monitored using an Omega FTB 793 flow meter. A reference fuel (Indolene) was used in the experiments. Vapor pressure, density, and viscosity were measured for the test gasoline and included in the CFD.

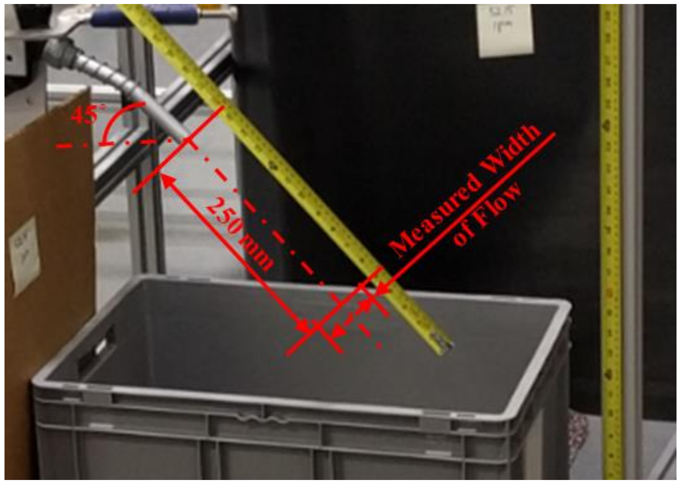

Figure 4.2 Experimental setup for the spray width measurements

4.1.1.2 Air Entrainment Measurement

As a part of the shut-off mechanism, refueling nozzles are designed to entrain air into the fuel while dispensing. The entrained air can alter the properties of the fuel mixture and affect the downstream dynamic behavior of the fluid. It is important to utilize appropriate entrainment values and air/fuel volume fractions in the CFD simulations to predict the nozzle outlet conditions. The air entrainment rate is experimentally measured and used to create an appropriate inlet boundary condition for the nozzle. A flow meter connected to a 3D printed collar, which sealed the air entrainment orifice located near the exit of the nozzle, was used to carry out the rate of air entrainment measurements as a function of fuel flow rate. This data was used to determine what fraction of fluid flowing through the nozzle is gasoline and what fraction is air for a given pumping flowrate to be used as inlet conditions in the CFD simulations. The resistance of the flow meter was 500 to 650 Pa, which is small and was shown to have little effect on the flow rate measurements. Table 4.1 provides the air entrainment flowrate values at select fuel flow rates for the OPW 11B nozzle. These values agree well with previous work taken with different fluids and nozzle types[26].

Table 4.1 Air entrainment rates for OPW 11B

Gasoline dispense rate (GPM)	Air entrainment rate (GPM)	Volume Fraction of air at mass flow inlet
4	0.59	0.15
6	0.65	0.11
8	0.72	0.09
10	0.75	0.08

4.1.2 Simulation Setup

To visualize the nozzle spray and compare with experimentally measured spray patterns, simulations were set up to capture a 250 mm long exit domain, which was modeled in the shape of a cone, extending from the outlet of the nozzle. Run time of simulation is set to 1 sec such that a steady state solution is achieved, determined by mass conservation. The external geometry domain is depicted in Figure 4.3

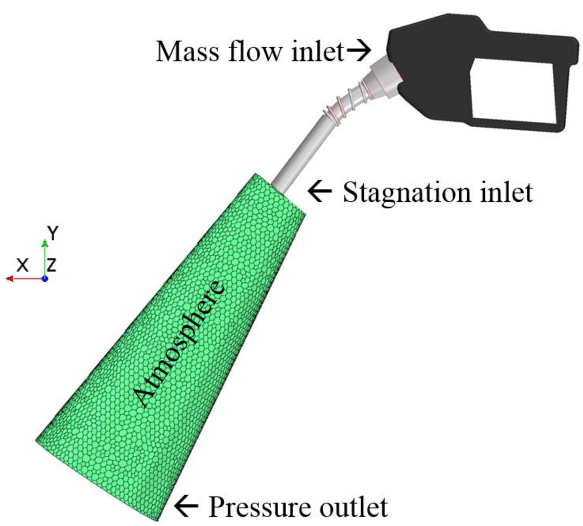

Figure 4.3 Simulation setup depicting the external CFD domain

The base size of the mesh along with custom volumetric controls was set such that the meshing continua keeps the Courant Number below 1. More information about the simulation is given in the Table 4.2 below.

Table 4.2 General Nozzle Simulation Information

Density of fluid [kg/m^3]	Dynamic Viscosity of fluid [Pa-s]	# of Cells	Mesh Base Size [mm]	Time Step [s]	Average CCN	# of Cores Used	Time to Compute [hrs]
746.40	4.0942 x 10^{-4}	43204 for nozzle 490957 for atmosphere	1.44 to 4	0.0001	0.63395	256	~1hrs

4.1.2.1 Geometry Creation and Nozzle Function Description

Two gasoline nozzles were used in this study, one manufactured by OPW (OPW 11B) and the other by Husky (Husky X1). Both nozzles were recreated as 3D CAD models by dimensioning the dismantled nozzles using a digital caliper with measurement tolerances of ± 0.05 mm.

The geometries of the Husky and OPW nozzles are shown in Figure 4.4. Both nozzles are similar in construction, in that each has a spring check valve at the top of the nozzle insert (1) and an internal plastic tube running the length of the nozzle (2). The pressure ports (3) are holes located on the bottom of the nozzle near the tip that draw air in from the filler pipe during operation. This allows a poppet valve (not shown in diagram) to stop the flow of fuel when this pressure port is covered with fuel, e.g., when refueling has finished. Both nozzles have similar obstructions directly behind the check valve (1) in the form of a pillar and internal airflow passageway channels to direct the entrained air into the fuel flow stream. The final fuel flow obstruction as a result of the entrained air inlet is unique in each case; it is present near the tip of the nozzle in the form of a structure in both nozzles that funnels the pressure port into the internal tube. For the OPW nozzle, this structure consists of a small rectangular block (4), while in the Husky nozzle it consists of three equally spaced fins (5). This final obstruction was seen to contribute to significant differences in the spray pattern observed in both experiment and simulation between the two nozzles (shown later). For the OPW 11B nozzle, the funneling element, rectangular block is attached to the inner wall of the nozzle and is asymmetric. The asymmetric nature of the block causes flow to fan out more. For Husky, the funneling element is symmetrical in nature, which gives a jet-like flow. It is a three fin structure and one of the fins is attached to the pressure port providing a path for entrained air to travel from the port to the plastic tube.

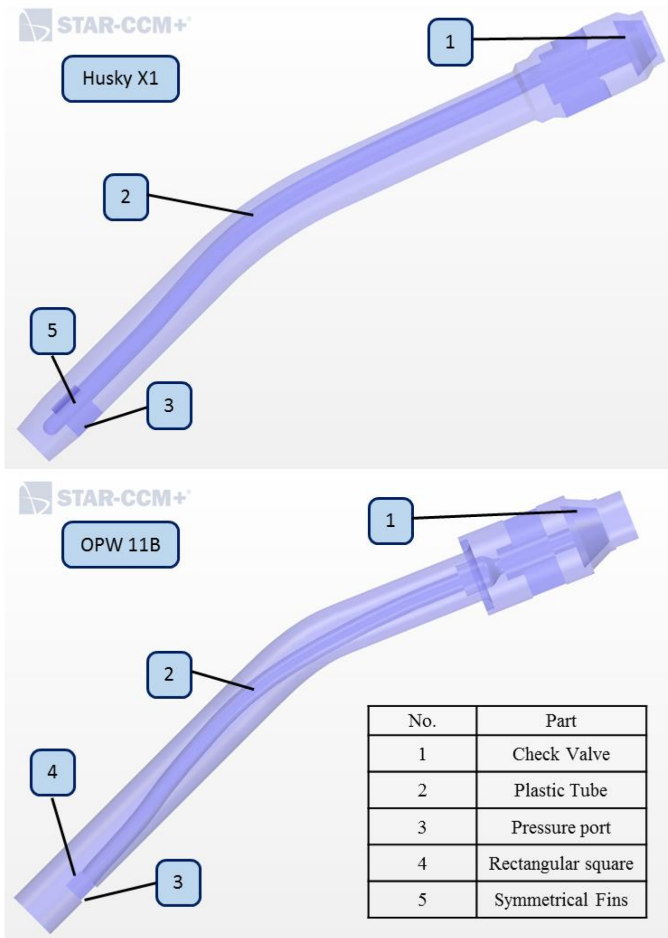

No.	Part
1	Check Valve
2	Plastic Tube
3	Pressure port
4	Rectangular square
5	Symmetrical Fins

Figure 4.4 Recreated internal geometry of Husky X1 (top) and OPW 11B (bottom) nozzles

For these simulations, the inlet (fluid supply) conditions were set to match measured flowrates and consisted of homogenous mixture of air/gasoline with corresponding volume fraction matching those from the air entrainment measurement (Table 4.1). Simulation consisted of modeling the nozzle assembly (depicted in Figure 4.4) that extends out of the main body and handle. The CAD geometries used for the CFD domain were created using PTC Creo Parametric, from dimension measurements taken of the deconstructed nozzles. These geometries were surface repaired manually in STAR CCM+.

4.1.3 Refueling nozzle characterization results

Simulations were carried out using the full geometry which included all the internal flow features up until the check valve of the nozzle. In This section, results of those simulations are presented.

Figure 4.5 shows how the spray width changes as a function of fuel flow rate in both the CFD simulations and the experimental measurements for each nozzle type. Overall, the spray patterns of both nozzles show good agreement and follow the patterns of experiments when fuel flow rate is increased (less than 12.5% deviation for OPW and 17.5% for Husky). For the OPW nozzle, the spray was seen to spread more with higher flow rates because of the impedance of the rectangular block, a component of the air entrainment assembly. This pattern was not seen in the Husky nozzle as the funneling element located at the end of the nozzle body is more symmetrically designed to allow the fuel flow to pass with less obstruction. As such, there was almost no difference in spray characteristics between 4 to 10 GPM.

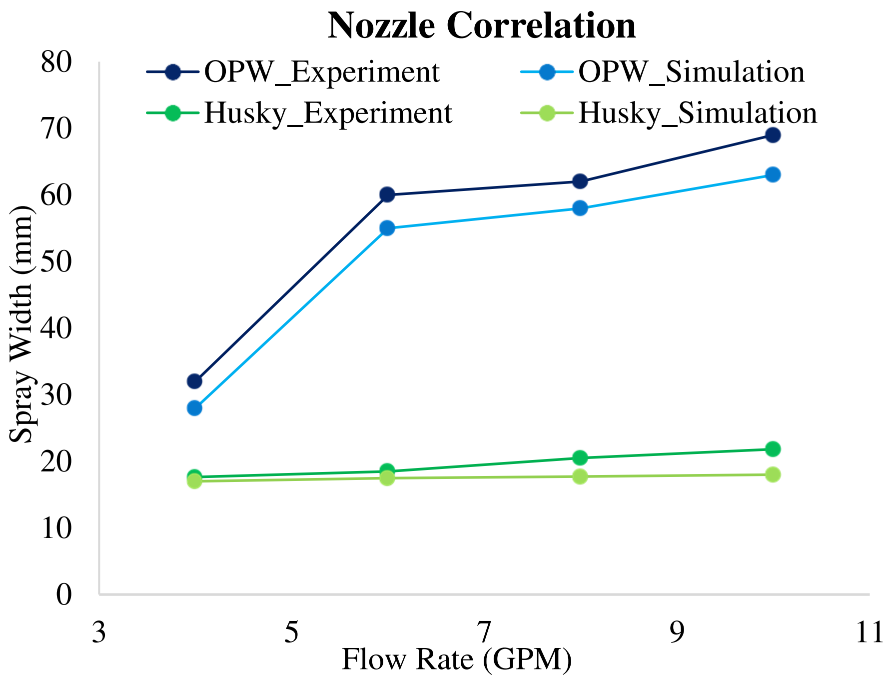

Figure 4.5 Comparison of the fuel flow rate dependent spray widths for two nozzle type

It is obvious that the internal nozzle geometry, especially for the OPW 11B nozzle, can largely affect the fluid dynamics, which control the outlet flow conditions. Photos from experiments and scenes from simulations at various flow rates for each nozzle are provided in Figure 4.6 to Figure 4.9.

Figure 4.6 OPW11 B at different flow rates: Experiment

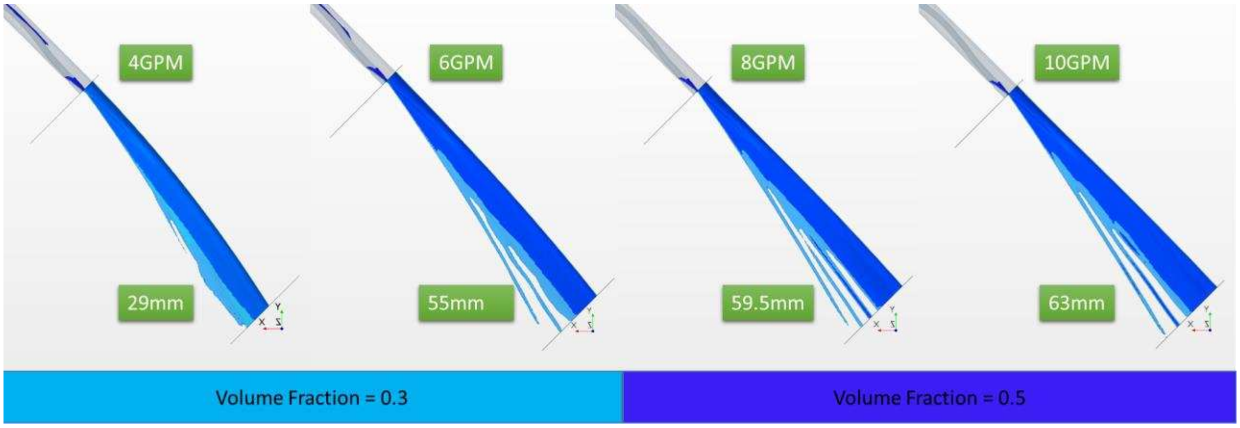

Figure 4.7 OPW11 B at different flow rates: Simulation

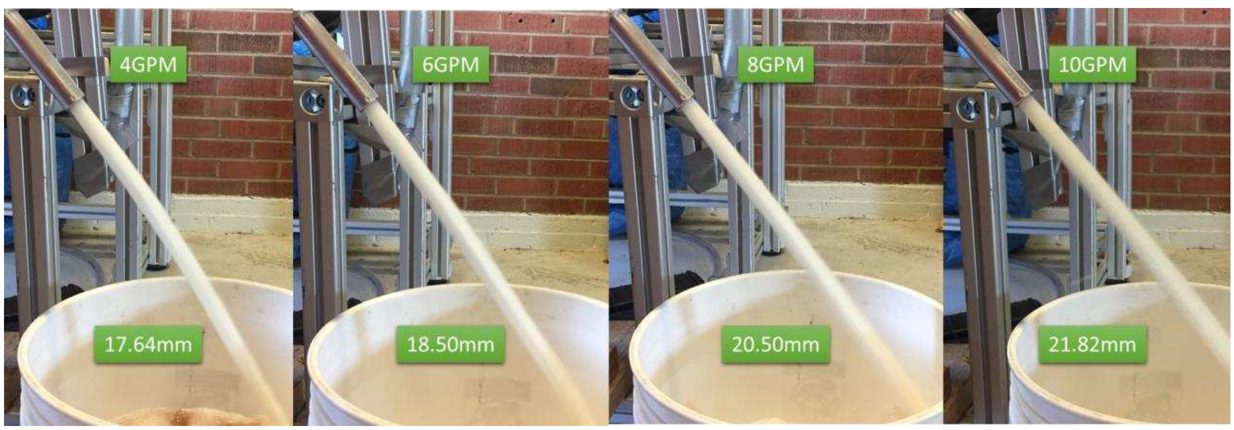

Figure 4.8 Husky X1 at different flow rates: Experiment

Figure 4.9 Husky X1 at different flow rates: Simulation

4.2 Boundary 2 – Stagnation

The refueling system in this study has a fillerpipe with a capless module. This means the operator does not have to turn open a cap before refueling. Refueling can be started just by pushing the nozzle into the fillerpipe. When the nozzle is inserted into a fillerpipe (normal refueling operation), some amount of opening around the nozzle of the fillerpipe is open to atmosphere. This condition is modeled as a stagnation boundary. The reference pressure on this boundary set to zero. This means air can go in and out as per simulation requires. Outgoing phases can be fuel or air but incoming phases are set to air only. This boundary is shown in the Figure 4.10.

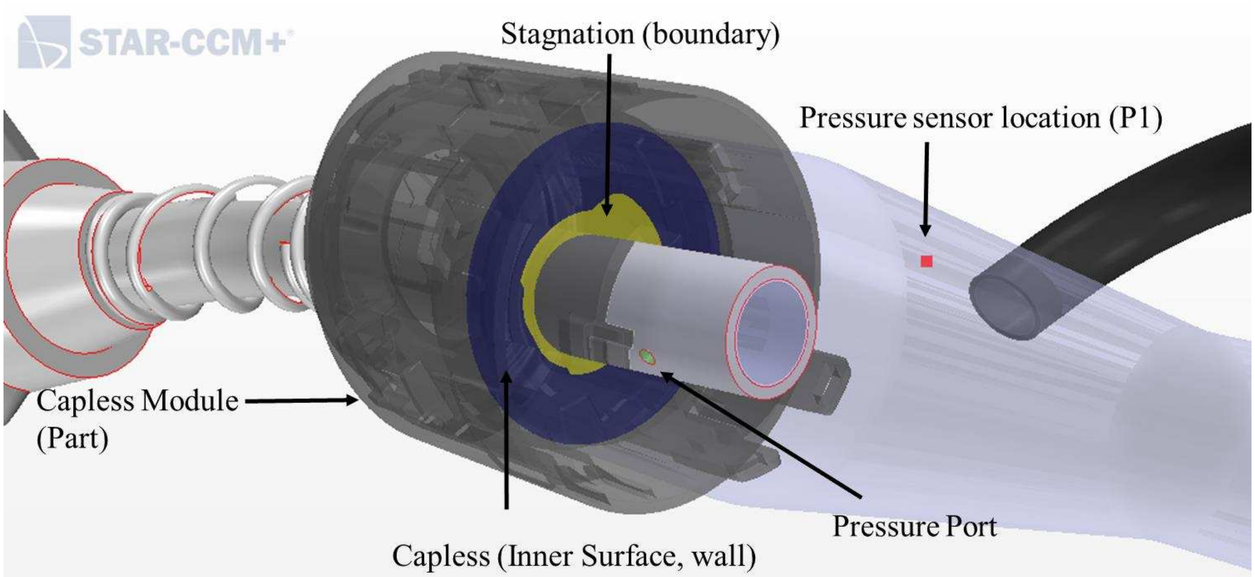

Figure 4.10 Location of stagnation boundary (colored yellow)

4.3 Boundary 3a and 3b – Vapor Return Line

Flow through the Vapor Return Line (VRL) is a crucial boundary condition for the model. The flow inside this line is driven by the pressure difference between tank and the opening of the fillerpipe. The restriction present in the line adds complexity. For different fuel flow rates the tank pressure is different, thus, for different flow rates of fuel there will be different flow rate of vapors in the vapor return line. To assist correlation between CFD and experiments, the characterization of the vapor flow through this part was carried out in Fort Collins atmospheric conditions. This characterization allows the VRL to be modeled as either an equation or table lookup. The intricacy in the VRL makes it too computationally expensive to model the actual geometry.

Figure 4.11 shows a schematic of how the VRL was tested. An Alicat Mass Flow Controller (MFC) was used. The flow straightener was a long section of PVC pipe. This was used to ensure fully developed flow. A manometer or pressure transducer was used to obtain the differential pressure across the VRL.

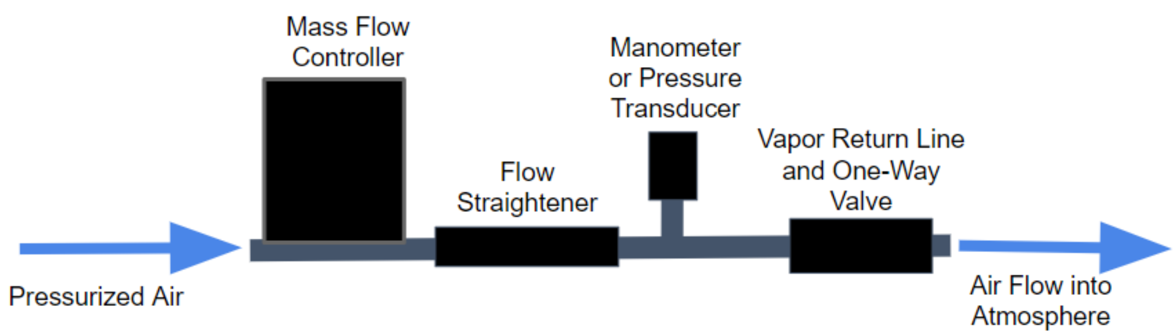

Figure 4.11 Schematic of VRL test

The compressed air and MFC were connected to the left end, the pressure sensor connected to the attachment near the right, and the VRL connected on the right end. The MFC was set to a specific flow rate and the system was allowed to steady. Then the corresponding differential pressure was recorded. The pressure transducers that are installed in the tank were used which have a ±6.67 kPa gauge pressure range.

Pressure drop versus flow rate was measured. Figure 4.12 shows the results of these tests. Flow rate is plotted as Standard Liters per Minute (SLPM). Standard conditions are 25°C and 1 atm ambient pressure. The ambient conditions for the tests were 21.2°C and 0.84 atm. The conversion to standard conditions is taken care of by the MFC; the flow rate of the MFC is set in

SLPM. A polynomial is used to fit that characteristic curve and this polynomial is used to define velocity magnitude at 3a (as ingoing) and 3b (as outgoing).

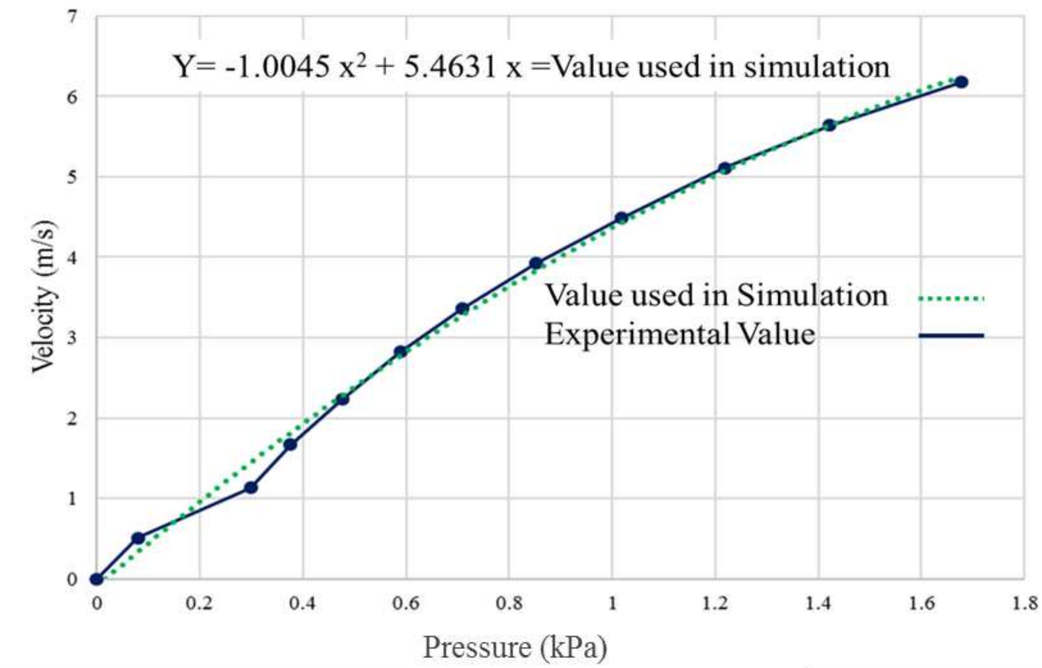

Figure 4.12 Experimental and value used in simulation of velocity for VRL

Using this method it is not necessary to mesh the VRL. Boundaries are set such that inlet and outlet of the vapor return line follow the trend shown by the dotted line for 90% of the tank filling, and after that, the value will become zero. This means no flow will flow through vapor return line after 90% of tank fill. This is because the tank is designed such that the VRL is completely closed after 90% fill. It can be clearly seen that at lower pressure drops the experimental values do not match the field function curve (at 0.3kPa). To avoid this in the future, a table input can be used instead of field function and values in between data points can be interpolated.

4.4 Boundary 4 – Canister Line

Flow exiting the tank through the canister line is another important boundary condition. In this case, the canister orifice is modeled geometrically in the CFD. The pressure versus flow rate data is used to confirm that the geometric model is capturing the canister line characteristics. Figure 4.13 shows the canister mimic orifice.

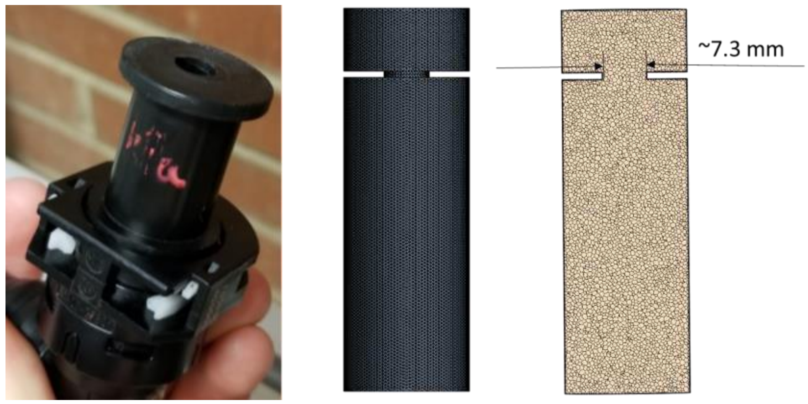

Figure 4.13 Canister mimic orifice

The test setup for characterizing the canister hose and orifice is identical to that used for the VRL and OWV. All components upstream of the part are the same; only the orifice and canister line are exchanged for the VRL and OWV.

The orifice can be modeled directly with actual geometry. Fortunately, the geometry for canister orifice (Diameter = 7.2 mm) is not overly complicated or small and can be modeled directly in the CFD without adding a noticeable amount of computation time. The canister orifice was solid modeled in SolidWorks, surface repaired in STAR CCM+, and attached to the canister line extending from the fuel tank. The base size of the mesh required for canister orifice is not smaller than the base size for nozzle, so the part can be meshed without modifying time step. Flow characteristic from the experiment and predicted with the simulations are shown in Figure 4.14. This method is used for the simulation because it is simple (will just need a CAD drawing whenever there is a change in orifice size).

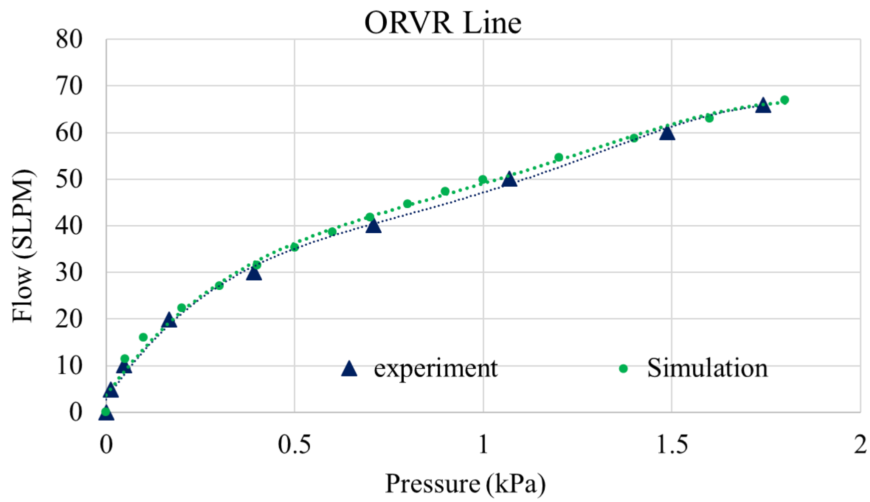

Figure 4.14 Canister line flow characteristics

5 Geometry Description

5.1 Introduction

3D CAD data for a refueling system (tank and fillerpipe) was received from Honda R&D Americas, Inc. This CAD data is from a production Honda vehicle. These geometries were imported in STAR CCM+ and prepared in order to mesh them. Details about these operations are given below.

In CAD design, two methods can be used to create a part. The first is solid modeling (neutral format .stp) where basic objects like cylinders, cones, etc. are used to make a desired object. The second is by way of surface modeling (neutral format .stl) where a user creates surfaces and patches them to make the desired object. Solid modelling is used for prototyping and product visualization whereas surface modeling is used for CAE and 3D printing purposes[26].

Neutral file formats are used by every CAD software to facilitate geometry import and export. Parent CAD software is the platform where the geometry is created. In the parent CAD software, all the parameters and features such as construction lines, axis, dimensions, operations performed, etc. are present. When a geometry is exported out of a parent CAD software using neutral file formats and imported elsewhere, it loses those parameters and features.

In order to use a solid modelled (.stp) geometry for CAE purposes it requires conversion to a surface modelled geometry (.stl), so that a surface mesh may be applied. Alternatively, one could create a surface modelled geometry in the first place. Nevertheless, for such a conversion, there are several stand-alone software packages capable of doing this, including STAR CCM+. However, issues can arise when this conversion is performed. The following criteria must be met before a geometry can be meshed (or used for CAE):

1) Surface should be a closed manifold

2) None of the surfaces should intersect with one another

3) Surfaces should not have free edges

To meet these conditions the built in surface repair tool in STAR CCM+ is used in this study.

5.2 Fillepipe Surface Corrections

Filler pipe geometries available are solid modelled geometries. Surface repair tool has been operated on those geometries to remove errors like pipe thickness, hole inlets/outlets. Figure 5.1 compares a geometry before and after surface repair.

Figure 5.1 Comparison between geometry before (left) and after (right) surface repair

5.3 Nozzle Orientations

Refueling systems have to be tested for different orientations of nozzle with respect to fillepipe to pass marketability requirements. As the orientation of nozzle with respect to fillerpipe changes the performance of the system changes. Therefore, in order to capture the performance of the system correctly the correct orientation of the nozzle with respect to fillerpipe (angle that nozzle makes with the fillerpipe) should be correctly modelled. The methods used to achieve correct orientation in CFD is discussed in this section.

The surface repairing techniques are used for repairing the nozzle geometries after being created in Creo Parametric. When nozzle and filler neck geometries are imported in STAR CCM+ with help of .stl neutral formatting from their parent CAD software (Creo for nozzle and CATIA V5 for the filler neck), the geometries do not contain any features or orientation parameters associated to them. This requires two separate coordinate systems (one for nozzle and another for filler neck) to be co-aligned to create the proper nozzle/filler pipe orientation, a highly difficult and time consuming process to achieve accurate orientation.

To alleviate this process, the surface corrected geometry file of the nozzle were successfully imported in CATIA V5 and merged/orientated in CATIA V5 itself. As CATIA V5 is the parent CAD software of the filler neck, the construction lines, axis, dimensions, etc. could be used as reference points/data to accurately position the nozzle within the filler pipe. Elasticity of the capless geometry, displacement of capless with respect to the filler neck and displacement of the internal parts within the capless module with respect to the fillerpipe have been neglected in nozzle/fillerpipe positioning practice.

5.4 Fuel Tank

When the full system geometry is checked for surface errors, the surface repair tool detected over a million errors requiring correction before meshing could be carried out (Figure 5.2, shown in red). Surface repairing to correct these errors takes a lot of time if done in STAR CCM+. The errors resulted from fittings, mountings, collars, caps, thicknesses, complex geometry and some parts that intersect each other. Mostly, these errors originate from parts or surfaces, which are not in the fluid region. This problem can also be solved by extracting the largest internal volume using CATIA V5. STAR CCM+'s Surface Wrap can also extract the largest internal volume with some limitations. For the simulations in this section, a Surface Wrap tool (a built-in tool in STAR CCM+) have been used on with specific volumetric and gap closure controls to extract the fluid region free from the surface. This tool acts as if a Saran^{TM} wrap is applied on the geometry to get the largest internal or external volume.

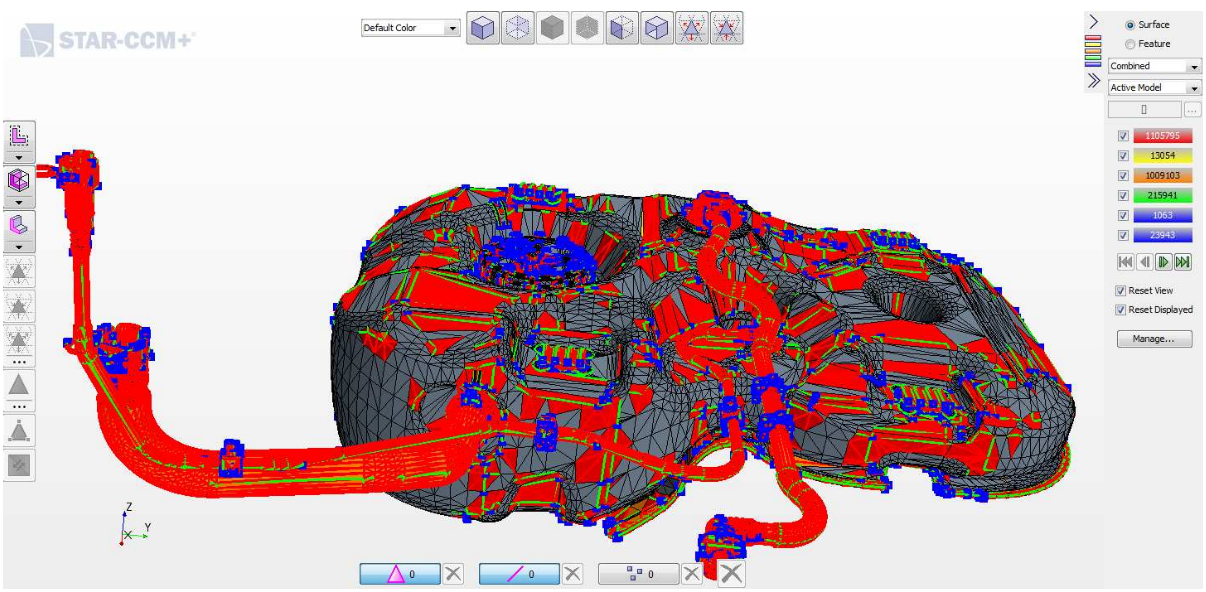

Figure 5.2 Surface errors present on the tank

5.5 Check Valve Opening

A check valve is present at location where the fillerpipe meets the tank. This part, which seals the tank volume from the atmosphere normally remains closed when not refueling. The check valve prevents vapors from climbing up the fillerpipe and escaping in to the atmosphere. Measurements were taken from the deconstructed tank to determine the liftoff clearance of the check valve so that the fluid dynamics through the check valve could be accurately modeled. Images of the check valve and measured lift is shown in Figure 5.3.

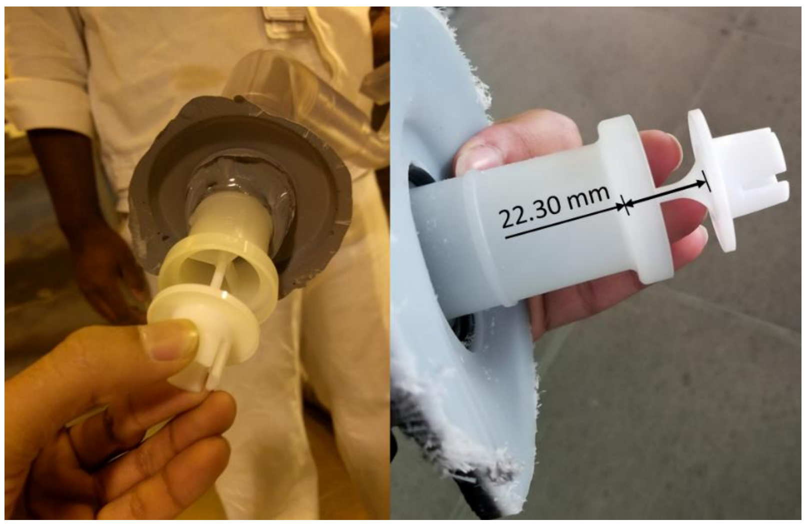

Figure 5.3 Check Valve Opening

To open the valve in the CFD model, a new coordinate system was created with the Z-axis pointing in the direction of the valve stem displacement. The actual opening is measured to be 22.30 mm. Geometry has been set up appropriately using a local coordinate system as shown in Figure 5.4.

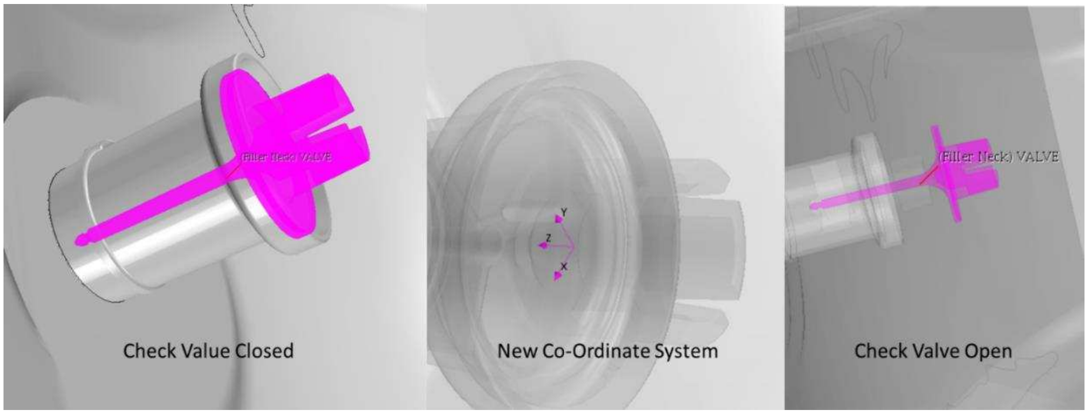

Figure 5.4 CAD view of check valve

6 Experiments and CFD Results Part – I: Refueling Nozzle and Fillerpipe

6.1 Introduction

The early click-off of the nozzle can be because of two main reasons; the back pressure of the tank and the recirculation of fuel at the upper part of the fillerpipe. The recirculation within the fillerpipe can happen in such a way that it covers the pressure port of the nozzle, thus shutting it off. In addition, if pressure inside the tank is high, the liquid level in the fillerpipe can flood the pressure port and cause the nozzle to shut off. In this chapter, focus is on the recirculation in the upper part of the fillerpipe. Only the fillerpipe and the nozzle make up the simulation domain[27]–[32]. General information about the simulation domain is given in the Table 6.1

Table 6.1 General Information about Part-I Simulations

Case Name	# of Cells	Mesh Base Size [mm]	Time Step [s]	# of Inner Iterations	# of Cores Used	Time to Compute [hrs]
NR85Go	625224	1.44 to 4mm	0.0001	10	256	~8hrs

6.2 Experiments Part – I

6.2.1 Experimental Setup

Honda R&D provided two fillerpipes (17660FE2PA000 FFP and 17660FE2PA100 FFP). These two fillerpipes will be called NoGo and Go respectively for convenience based upon experiments performed. For reference, these two pipes are shown below in the Figure 6.1.

Figure 6.1 Fillerpipes from Honda R&D

Experiments were performed to determine if/when early click-off occurred. The only change was that the fuel was flowing into a bucket instead of the fuel tank as the focus was on the early click-off because of the fuel recirculation. Additional data in the form of pressure traces and visualization were taken to further validate the CFD results. There are 14 different nozzle positions for performance testing. The fillerpipe was correctly mounted on a fixture in the identical orientation of that in the CFD simulations with respect to the direction of gravity. This can be seen in Figure 6.2. The side view and front view of the filler neck from STAR CCM+ is overlapped on the photo with the experimental setup to ensure the filler neck is mounted correctly. Three pressure sensors are mounted on the filler neck at the locations identified as P1, P2, and P3.

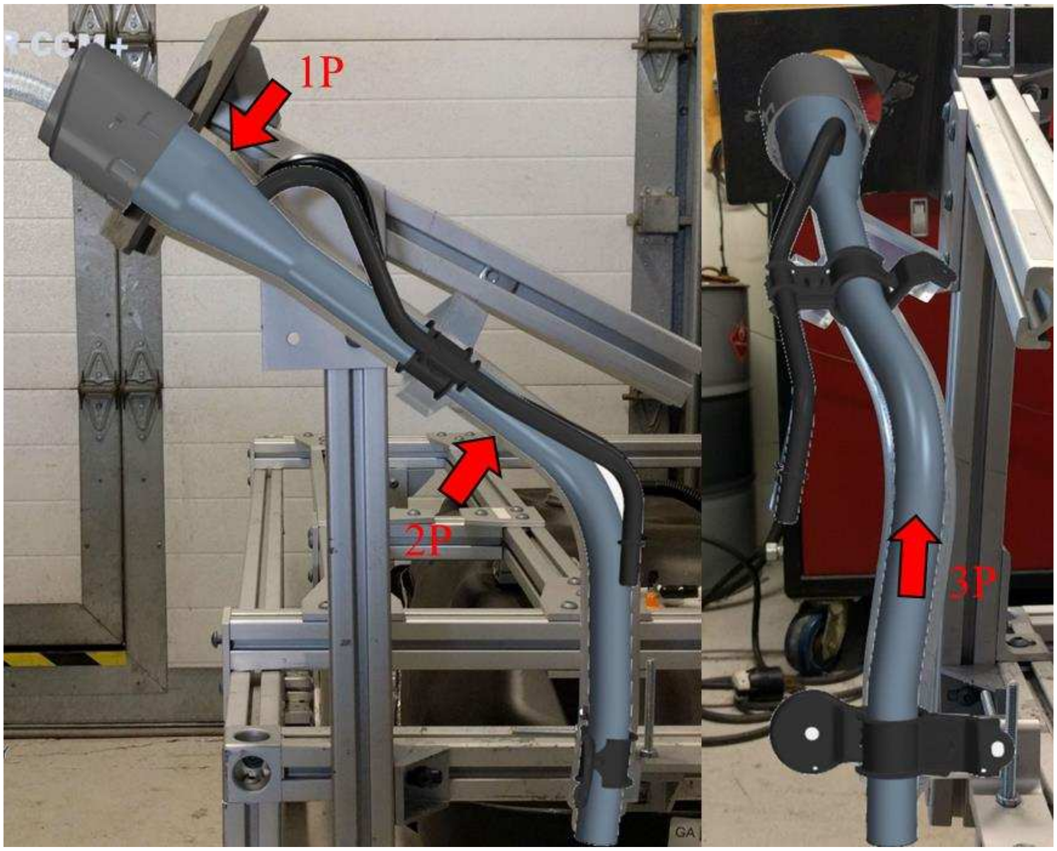

Figure 6.2 Side and front view (CFD geometry overlaid on experiment) and pressure sensor positions

Refueling testing is done for different nozzle orientations for each pipe. All 28 tests cases were filmed from side and front views using high speed videography at 240 fps. A bucket is used to collect the Indolene (test gasoline fuel) as it dispenses from the bottom of the filler neck[27], [33].

6.2.2 Experimental Results

Figure 6.3 shows pass/fail results from the set of experiments carried out on the two filler pipe designs according to the CSU’s performance testing procedures (14 different nozzle positions for each fillerpipe). Different nozzle orientations are set such that it incorporates general public behavior at a gas station. In each test, the nozzle is open and supplies fuel for 5 seconds. The flow rate was set at 9.85 GPM, the maximum achievable flow rate with the fuel cart at the time of testing. None of the fillerpipes demonstrated rise in liquid level during the first 5 seconds as there was not back pressure from the fuel tank. Each case was ran at least 3 times to test for early click-off. In four cases, early click-off is observed. Naming convention is as follows: L, R, or NR represents a 45° rotation either to the left (L) or to the right (R), or no rotation (NR), respectively. The following number represents the insertion depth of the nozzle in the fillerpipe (either 80, 85, 100, 120, or 127 mm) and the Go or NoGo represents the filler pipe being tested. For example, the L80NoGo specifies the test condition for a 45° rotation to the left with an 80 mm insertion depth into the NoGo filler pipe.

Test Case	Result	Percent Fail	Test Case	Result3	Percent Fail
L80Go	pass	0	L80NoGo	fail	50
L100Go	pass	0	L100NoGo	fail	80
L120Go	pass	0	L120NoGo	pass	0
L127Go	pass	0	L127NoGo	pass	0
NR80Go	pass	0	NR80NoGo	pass	0
NR85Go	pass	0	NR85NoGo	pass	0
NR100Go	pass	0	NR100NoGo	pass	0
NR115Go	pass	0	NR115NoGo	pass	0
NR120Go	pass	0	NR120NoGo	pass	0
NR127Go	pass	0	NR127NoGo	pass	0
R80Go	pass	0	R80NoGo	fail	40
R100Go	pass	0	R100NoGo	fail	20
R120Go	pass	0	R120NoGo	pass	0
R127Go	pass	0	R127NoGo	pass	0

Figure 6.3 Experimental test results for different nozzle orientations

Failing cases R80NoGo, R100NoGo, L80NoGo and L100NoGo were re-tested 10 times. It was seen that failing does not occur every time a test is carried out. Variability in the tests can be attributed to a couple of uncertainties including the transient fuel flow rate delivery from the fuel cart, as well as slight variability in nozzle positioning from test to test.

6.3 Simulations Part – I

6.3.1 Monitor setup

Five monitors are set up in the simulation to monitor the fuel flow dynamics and quantify a particular case's tendency to click-off. Three of them are for pressure (locations of which are identified in Figure 6.2), the fourth is for measuring 'Surface Average' of volume fraction of Indolene on the inner surface of the capless module, and the fifth for measuring 'Surface Average' of volume fraction of Indolene on the pressure port surface located on the bottom of the refueling nozzle. The last two monitors are used to quantify the predicted liquid fluid recirculation, which is responsible for nozzle click-off in the physical experiments. In Figure 6.3, the navy blue colored surface represents the inner surface of the capless module; the green circle illustrates the locations of the pressure port on the nozzle; and the red square is the location of the first pressure sensor. The location of other pressure sensors (P2 and P3) can be seen in Figure 6.2. The yellow surface shown is the shape of the second sealing flap in the capless module. In the simulations, a stagnation boundary condition is applied over this surface, allowing air to freely come in or go out through this surface as per the fluid dynamics of the system.

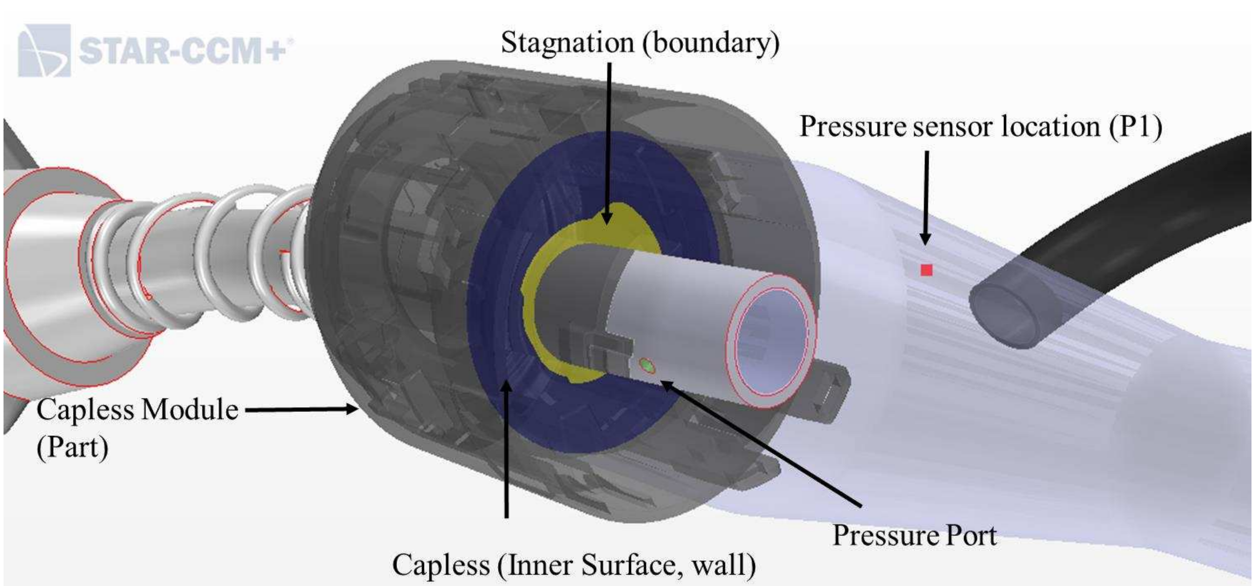

Figure 6.4 Monitor Setup

6.3.2 Part – 1 Simulation results

6.3.2.1 Pressure Data

The correlation of pressure data from NR85Go test case, a representative case, are shown in Figure 6.4. The average of the experimentally measured pressure at P3 is 0.256 kPa compared to the average predicted value of 0.299 kPa. The positive pressure is a result of the Indolene hitting the P3 sensor with large momentum. In this case, the P1 monitor pressure traces from both simulation and experiment indicated negligible pressure changes.

For the second pressure sensor, P2, a correlation has been seen in the trend of pressure between simulation and experiment, in that both indicate a pressure drop at similar times after the initiation of the flow. However, the difference of magnitude observed between the two signals is significant. The average of the experimentally measured pressure at P3 is -0.32 kPa compared to the average predicted value of -0.71 kPa. The overall trend of pressure values from experiment and simulation match each other. The pressure traces from experiment and simulation are shown in the Figure 6.5 below.

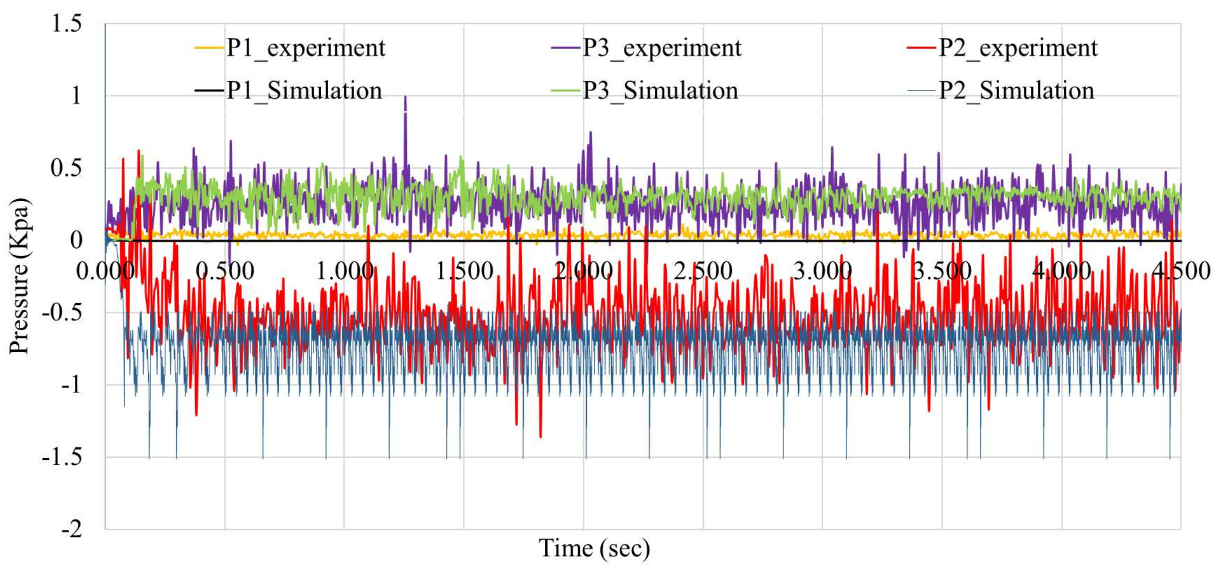

Figure 6.5 Pressure data comparison between P1, P2 and P3

6.3.2.2 Visual Correlation

The visual comparison between the 100 mm insertion rotated to the left for both Go (left) and NoGo (right) filler pipe cases including both CFD screen captures and still frames from the experiments are shown in Figure 6.6. The CFD screen captures are such that dark blue to sky blue represents 1 to 0.1 volume fraction in entire domain combined with a 0.5 volume fraction IsoSurface to identify the fluid stream exiting the nozzle. Early click-off is caused due to development of a pool from recirculated liquid. When this pool rises enough to block the pressure port of the nozzle, and click-off occurs. In the test case shown, the Go pipe did not experience click-off while the NoGo pipe did. It can be seen from both the CFD predictions as well as the experiments marked by the red arrow, significantly more liquid recirculation in the NoGo geometry compared to the Go design. Note the bubbly flow of Indolene causes the pool to look more significant in the experiments than the CFD.

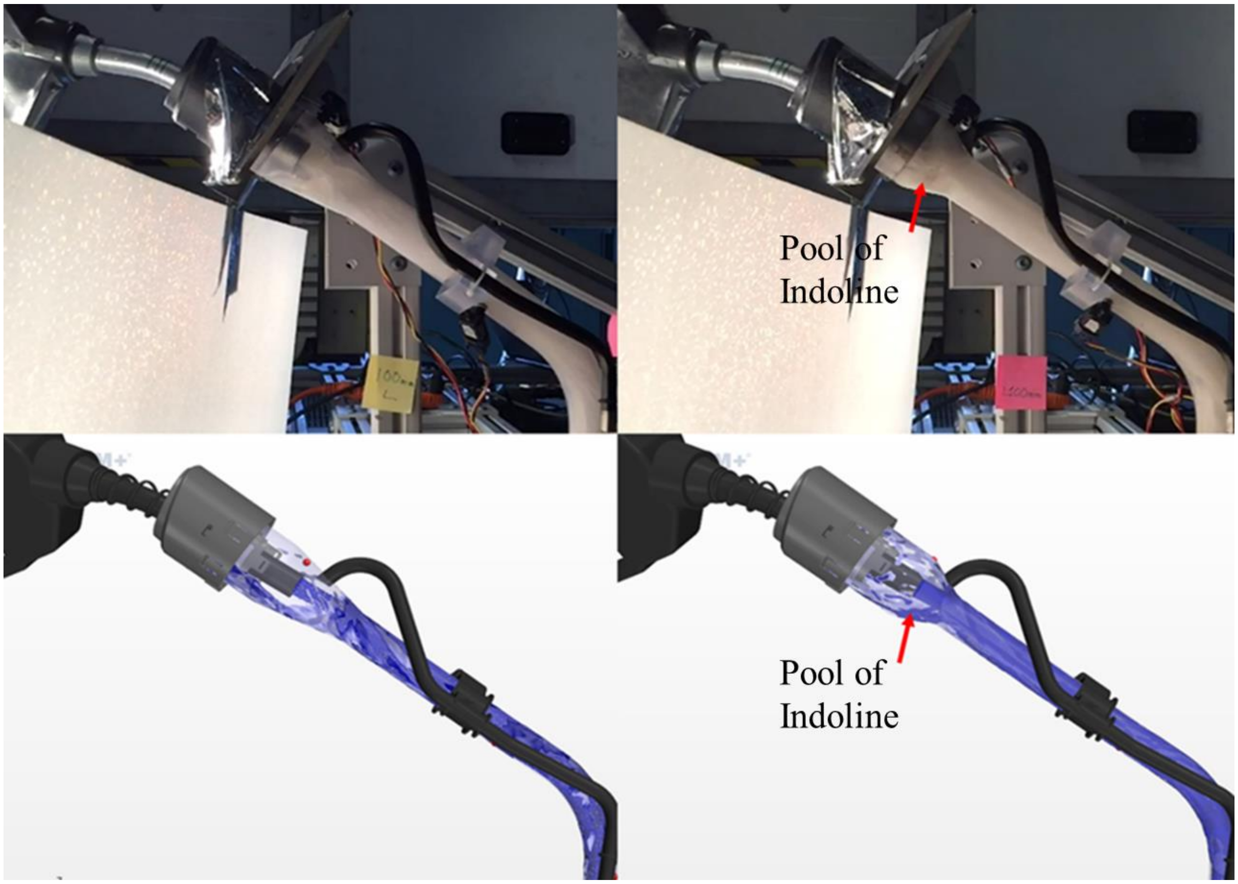

Figure 6.6 Visual Correlation between the Go (left) and NoGo (right) pipe

6.3.2.3 Click-off Prediction

In this section, as previously discussed, liquid mass accumulation is monitored in two locations in order to assess whether a design would lead to early click-off. Since early click-off occurs as a result from blockage of the pressure port of the nozzle, it was an obvious choice to monitor the amount of liquid mass that came into contact with this surface during the course of the simulation as an indicator for click-off. However, a model may predict liquid recirculation, which would be indicative of fluid pooling and click-off, but may not predict the exact location of the fluid and thus accurately predict the amount of fluid contacting the location of the pressure port. As such, it was also decided to monitor the entire inner surface of the capless module.

Sum Capless is a function defined in STAR CCM+, which calculates the total spatially averaged mass flow over the inner surface of the capless module during the course of the simulation. The methodology used to calculate its value is explained below:

a) Volume fraction of Indolene is calculated on every cell, which lie on the inner surface of the capless module (navy blue colored surface in Figure 6.3, termed as Capless).

b) Surface average is calculated as:

$$Surface\ Average = \frac{Sum\ of\ Volume\ fraction\ of\ Indolene\ on\ each\ face}{Number\ of\ faces\ on\ capless} \qquad \text{Eq 6.1}$$

c) The above value is calculated after every 0.0006 sec for 3 sec, thus giving 5000 values at the end of the simulation.

d) The summation of these 5000 values are plotted in Figure 6.7

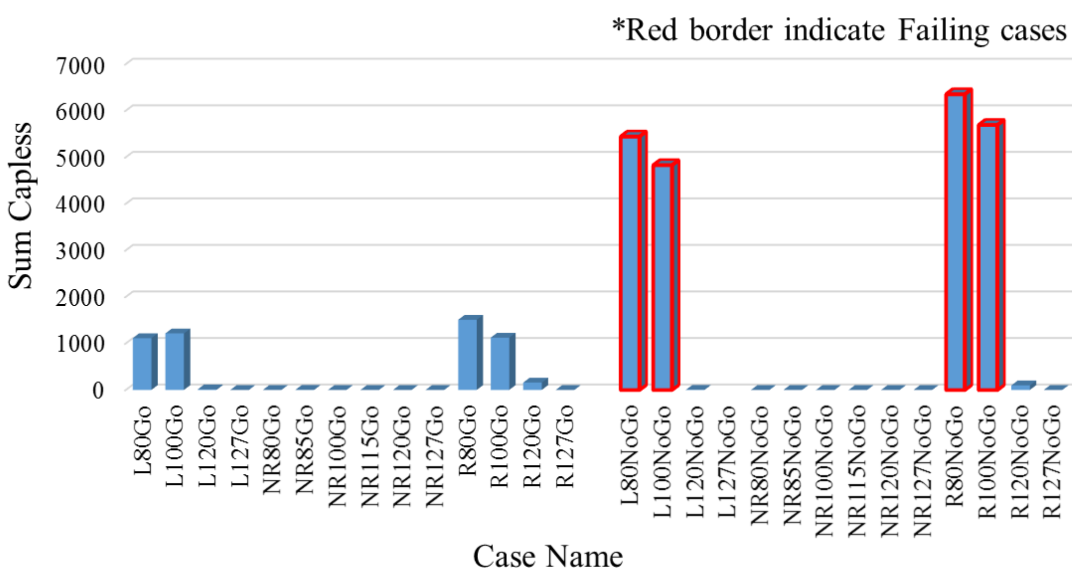

Figure 6.7 Sum Capless plotted for each of the test conditions

The Sum Port function defined in STAR CCM+ follows a similar process as that of the Sum Capless but calculates the volume fraction of Indolene for all faces which lie on the pressure port of the nozzle (green colored surface in Figure 6.3, termed as Port). The summation of the surface averaged volume fraction are plotted in Figure 6.7

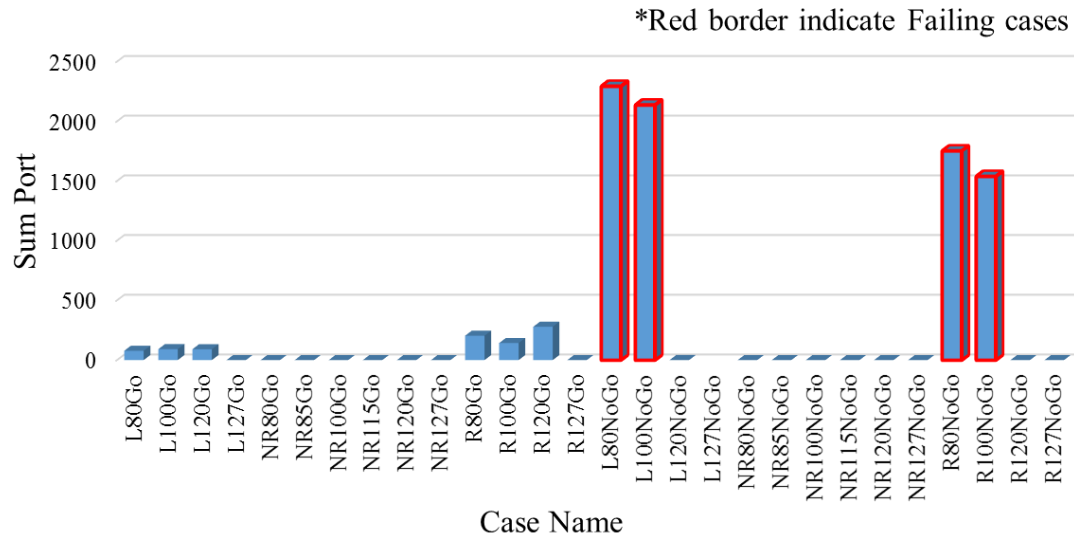

Figure 6.8 Sum Port plotted for each of the test conditions

Figure 6.6 and 6.7 indicate values for Sum Capless and Sum Port respectively for all 28 cases. It is very clear that the cases where nozzle is rotated either to left or to right at insertion of 100mm and 80mm are more likely to have liquid recirculation in the filler pipe. The Sum Capless and Sum Port values for NoGo filler pipe cases are 5 and 10 times more than the Go filler neck for these test conditions. As illustrated in Figure 6.3, the NoGo filler pipe when rotated to the left clicks-off more often than rotated to right. The sum port function predicts this trend as well. In this regard, for the cases explored here, the Sum Port surface summation value is a better criterion to decide whether a pipe will click-off or not.

Comparing the Sum Port predicted values shown in Figure 6.8 with experimental data, a conclusion can be derived for predicting click-off. If for a filler pipe the Sum Port value is more than 1500 in a 3 sec simulation (derived from R100NoGo) it will experience early click-off as a result of fluid recirculation. If for a filler pipe, the Sum Port value is less than 300 in a 3 sec simulation (from R120Go) it will not show any kind of early click-off. For values predicted between 300 and 1500, it is currently not possible to make any predictions and assign a confidence level. Additional filler pipes should be tested and simulated to add a confidence scale in this region.

7 Experiments and CFD Results Part – II: Full Refueling Assembly

7.1 Introduction

In this section, details about experiments and simulations are discussed when all the components present in a refueling system (tank, fillerpipe, nozzle, vapor return line and canister line) are considered. Experiments and simulations are carried out using a low vapor pressure fluid so that phase change can be ignored. The pressure inside the tank is monitored in experiments and provides the primary comparison to the simulations. Tank pressure is a highly important parameter as it can contribute to liquid level rise in the fillerpipe causing the nozzle to shut off and also drive vapors out of the fillerneck around the refueling nozzle which can lead to failed evaporation emissions tests.

7.2 Experiments Part – II

Pressure data obtained from filling the tank was one of the most important metrics for correlation with CFD. Pressure inside tank serves as an indicator of performance to developers of these refueling system. High pressure can cause early click-off whereas low pressure can cause spit-back. Pressure at several locations, flow rate, and ambient temperature data were collected using a data acquisition system. To measure flow rate a turbine flow meter from Omega is used (FTB-792: Repeatability: ±0.1% Pressure Rating: 1500 psig). The location of the pressure sensors on the tank is shown in Figure 7.1. Note that all pressures measured are gauge pressure. The influence of vaporization is neglected at this time and thus all filling tests and simulations were done with Stoddard fuel. Stoddard fuel has similar density and viscosity to gasoline, but has a very low vapor pressure allowing evaporation to be ignored in simulations. Table 7.1 shows the physical properties of Indolene and Stoddard fuel.

Table 7.1 Physical properties of Indolene and Stoddard fuel

	RVP (psi)	Dynamic Viscosity @ 25°C (mPa*s)	Density @ 25°C (g/cm3)
Indolene	9	0.413	0.749
Stoddard fuel	0.2	0.316	0.778

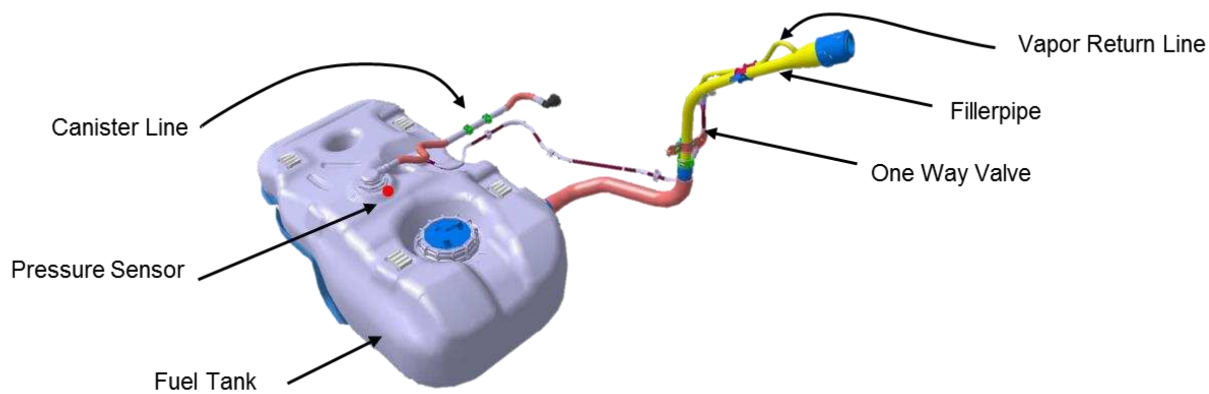

Figure 7.1 Location of pressure sensors on tank (red dot)

The primary pressure for correlation is obtained from the sensor next to the canister line. This will be referred to as the "tank pressure" in following graphs and tables. Figures 7.2 – 7.4 show pressure traces at this location for the tests run at 4, 10, and 14 GPM, respectively. These figures also display the flow rate measurements for the tests. A 20 Hz moving average filter was applied to the data prior to plotting[27].

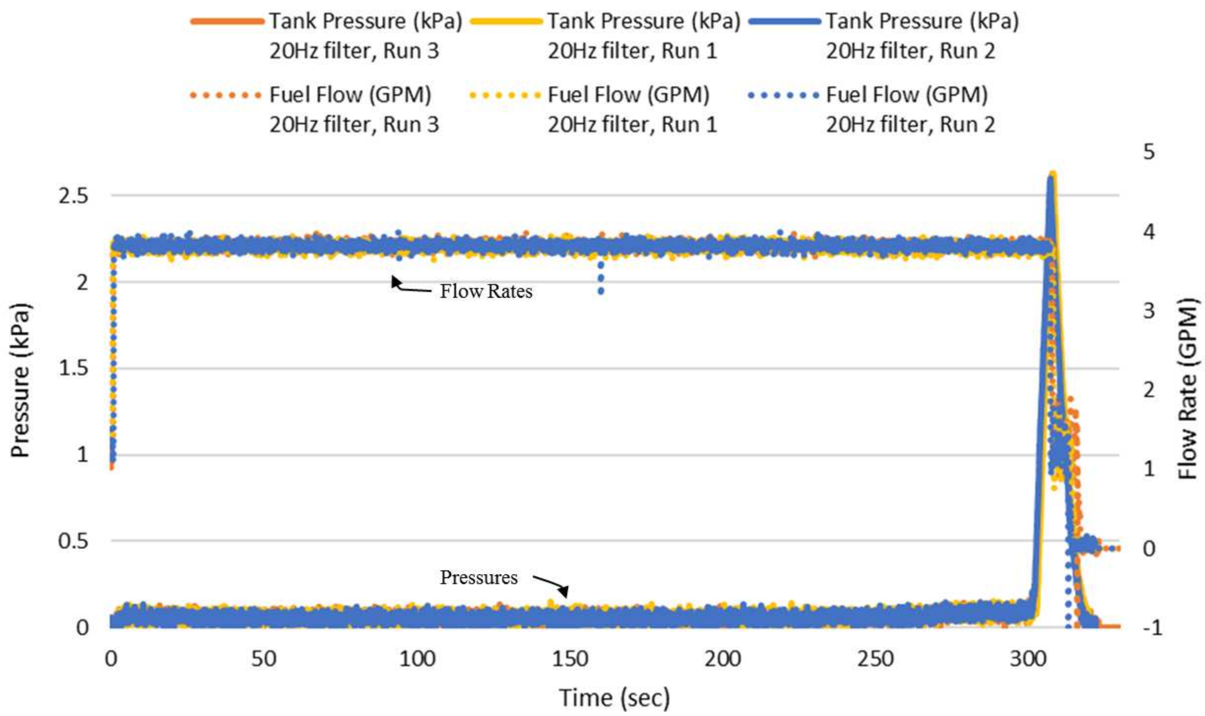

Figure 7.2 Flow rate and pressure traces for 4 GPM tests

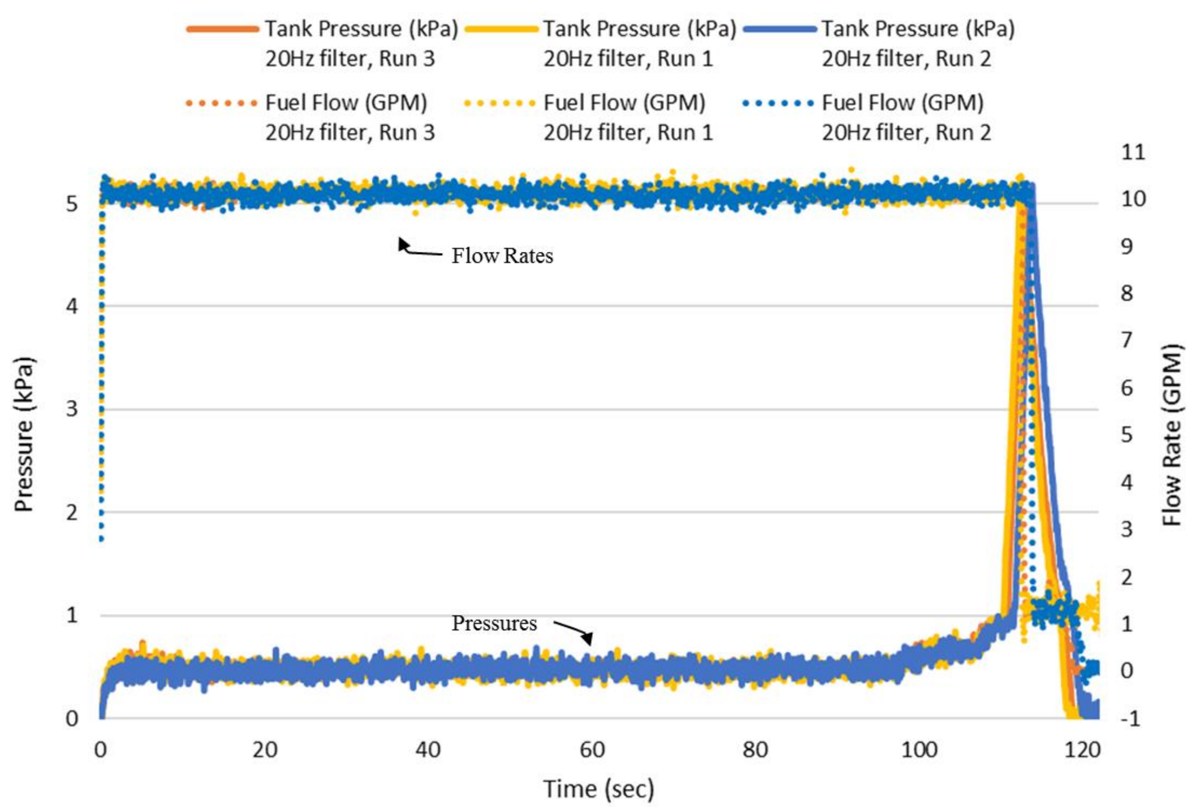

Figure 7.3 Flow rate and pressure traces for 10 GPM tests

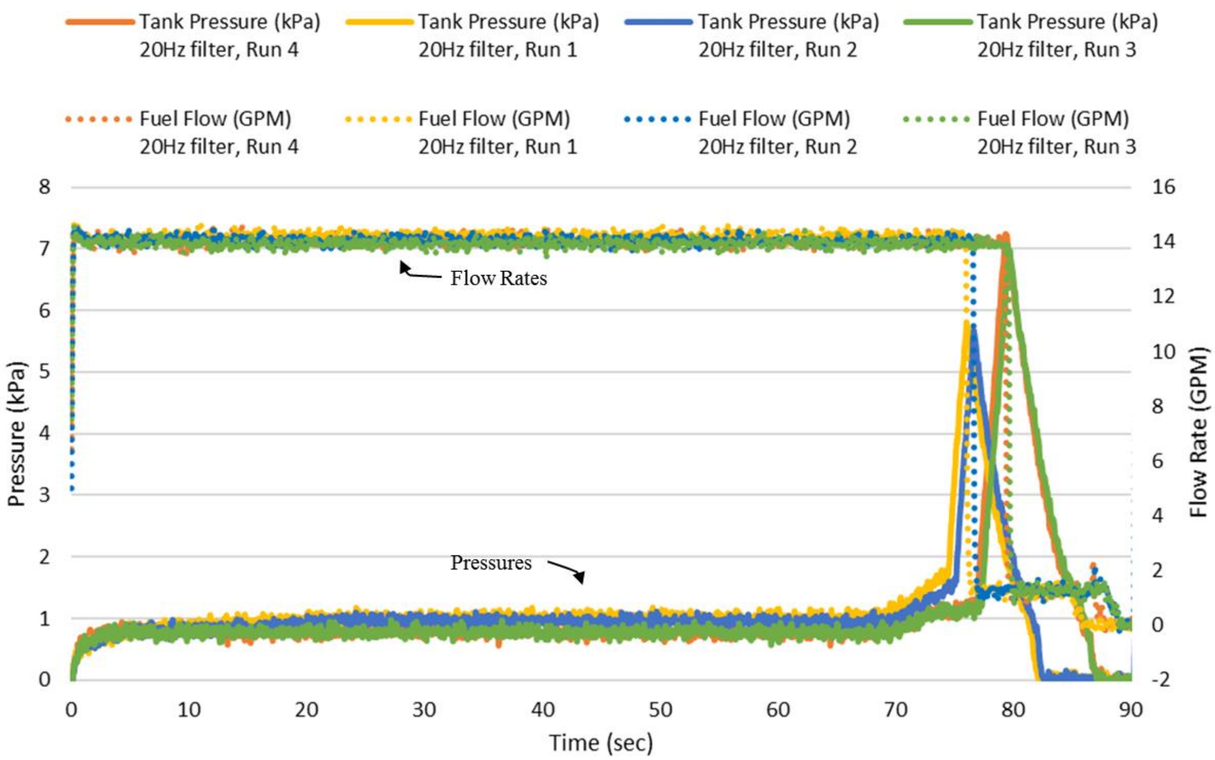

Figure 7.4 Flow rate and pressure traces for 14 GPM tests

The pressure spike at the end of the figures indicates nozzle click-off after the tank is full. The bump just prior to the spike is due to the VRL inlet closing. The overall trend indicates a steady state pressure rise and an increase in the magnitude of the pressure spike as fuel dispensing flow rate increases. The variability in the results arises from slightly different flow rates and slightly different prefill levels of the tank.

7.3 Simulations Part – II

The simulation domain contains entire refueling system with all the boundaries shown in Figure 4.1. General information about the simulations is given in the Table 7.2. Pressure inside the tank is monitored at every time step in the simulation with help of a point probe. The location of the pressure is shown in Figure 7.1.

Table 7.2 General Information about the Part-II Simulations

Case Name	# of Cells	Mesh Base Size [mm]	Time Step [s]	# of Inner Iterations	# of Cores Used	Time to Compute [hrs]
10 GPM	~2.2 M	1.44 to 4mm	0.0001	10	256	~3hrs (per sec of simulation time)

The following assumptions are made to simplify the CFD model:

1. Stoddard fuel is used in the experiments, which has negligible vapor pressure as compared to Indolene (0.02 psi vs. 9 psi). Therefore, phase change is ignored.
2. Temperature of the Stoddard fuel does not change in the simulation.
3. No solid continua for plastic body of the tank. Heat transfer between tank and fuel is completely neglected.
4. An exponential function is applied to account for the transient ramping of the fuel flow during the first 0.1 sec (i.e. flow rate ramps up from 0 to 14 GPM in 0.1 sec exponentially and remains constant after this initial startup)[11].

7.3.1 Part – II Simulation Results

Results of the simulations will be discussed in this section. Figure 7.5 shows the visuals from simulation as the tank fills. Visuals are created with help of scalar field (color bar) which indicates how much of the tank is filled (just on the wall of the tank, red is the level to which tank is filled) corresponding to a volume fraction shown on the color bar. The green colored cells represent a volume inside of the tank to see the spray pattern of the check valve. The cell in the cavity will become green if it has VF= 0.3 to 0.1, which represent bubbly flow[28].

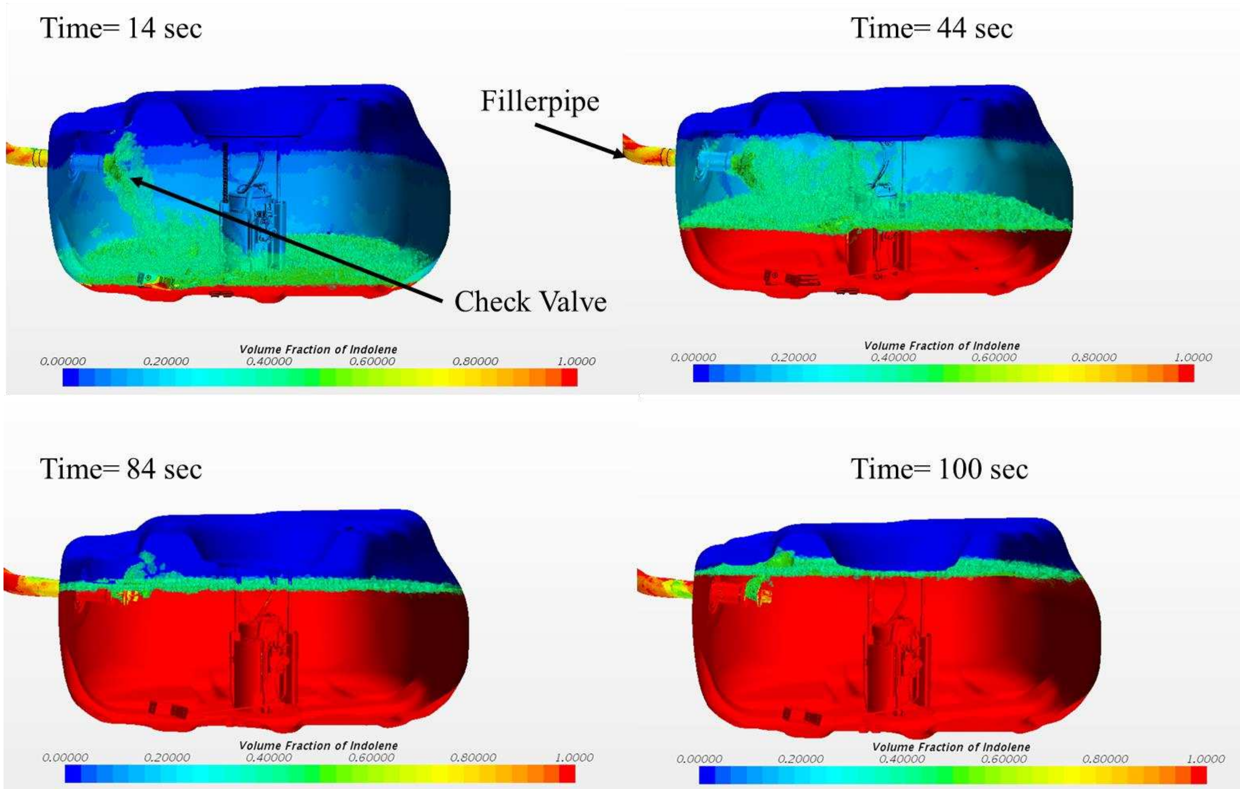

Figure 7.5 Filling of a fuel tank at 10 GPM

7.3.1.1 Pressure Data

A comparison of tank pressure shown by simulation and the measured pressure from a corresponding tank filling experiment is provided in Figures 7.6 to 7.8. The tank pressure after initial rise remains relatively constant. The 4 GPM case takes approximately 280 seconds to complete a fill. With the available computational resources, this would correspond to 35 days of computation. As such, the simulations were only run for 7 sec until a steady (level) pressure was noticed. The pressure spike indicates nozzle click-off. Figures 7.6 to 7.8 shows pressure spiking in simulation later than in the experiment. This is likely due to the slightly higher fuel flow rate during experiment and different prefill level in the tank. For all the simulations, the steady state pressure inside tank is slightly over predicted by the CFD by ~100 to 150 Pa. In the experiments after the closure of the VRL we see a pressure rise in the tank. CFD was able to capture this phenomenon as well.

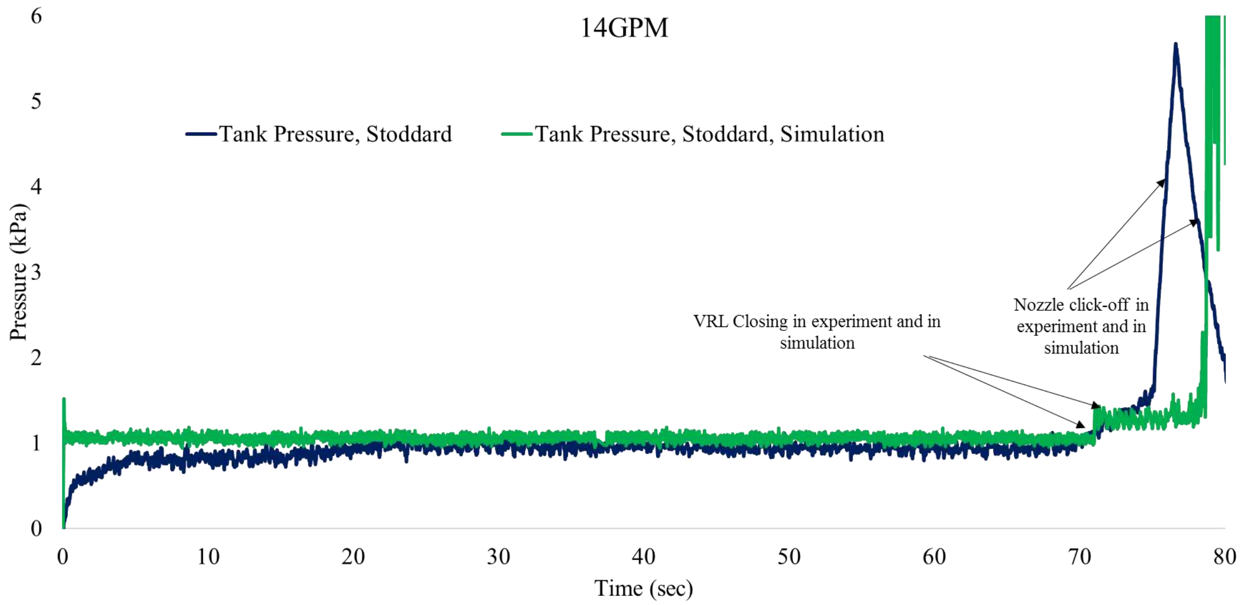

Figure 7.6 Tank pressure at 14 GPM

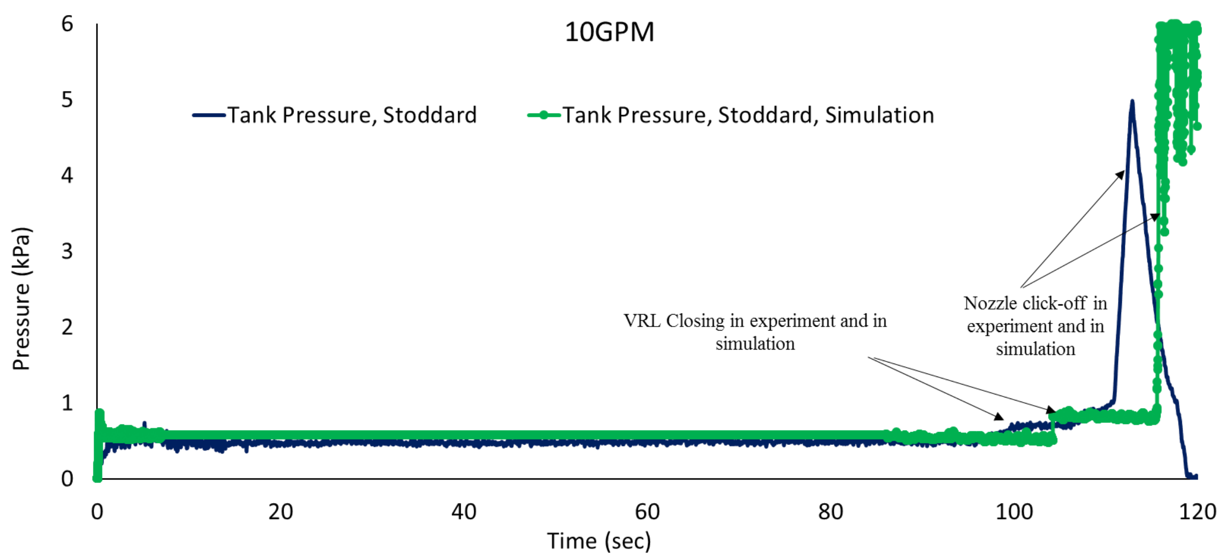

Figure 7.7 Tank pressure at 10 GPM

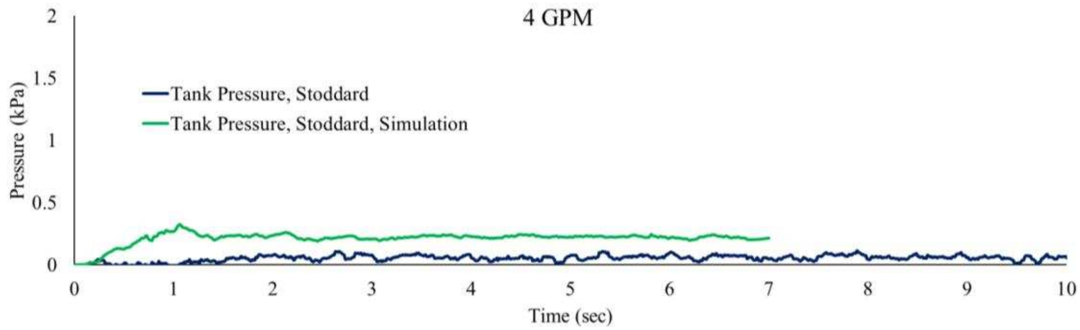

Figure 7.8 Tank pressure at 4 GPM

Figure 7.9 shows results for both simulation and experiments in more comprehensive way. The tank pressure trends the same as flow rate increases. However, pressure in the simulation is slightly higher than in the experiments at each flow rate. This shift varies from about 100 Pa to about 150 Pa. This magnitude shift is a positive result. It shows that CFD is able to predict steady state pressure in the tank if the shift is taken into account.

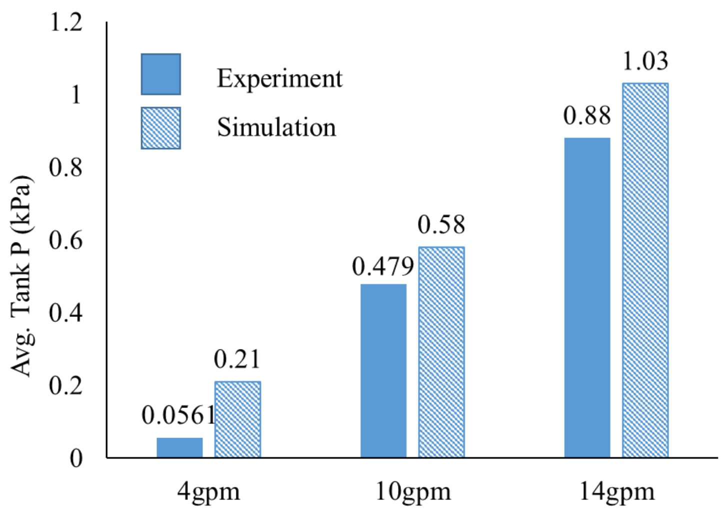

Figure 7.9 Pressure inside tank Simulation Vs Experiment

Table 7.3 shows results for both simulations and experiments in detail including the steady state averaged flow rates and the average standard deviation for both the pressure and flow rate measurements. It should be noted that the flow rates in the experiment are all slightly higher than used in the simulation. Flow rates are controlled by a ball valve in the experiments and the ball valve is difficult to set to maintain a constant desired flow rate.

Table 7.3 Average values from simulation and experiment

Flow Rate (# tests)	Average Tank P (kPa)	Approximate CFD values – Tank P (kPa)	Std. Dev. Of Tank P (kPa)	Average Flow Rate (GPM)	Std. Dev. Of Flow (GPM)
4 GPM (3 tests)	0.056	~0.210	0.019	4.12	0.043
10 GPM (3 tests)	0.479	~0.580	0.042	10.12	0.103
14 GPM (4 tests)	0.880	~1.030	0.115	14.07	0.162

7.3.1.2 Visual Correlation

In CFD, once the pressure inside tank peaks, the fuel level in the fillerpipe starts to rise and floods the pressure port of the nozzle indicating click-off. This phenomenon can be seen in Figures 7.10 – 7.13 where experiment and simulations scenes for 14 GPM case at different times are compared to one another. The simulation scene is created with help of resampled volume in STAR CCM+. The flow is airy and turbulent that is why it is very difficult to identify the surface. Volume resampling is a technique for rendering volume at a relatively low computational cost. A key element of this technique is the voxel, a pixel that represents volume in three-dimensional space. Each voxel has an opacity and color depending on the presence of liquid in it.

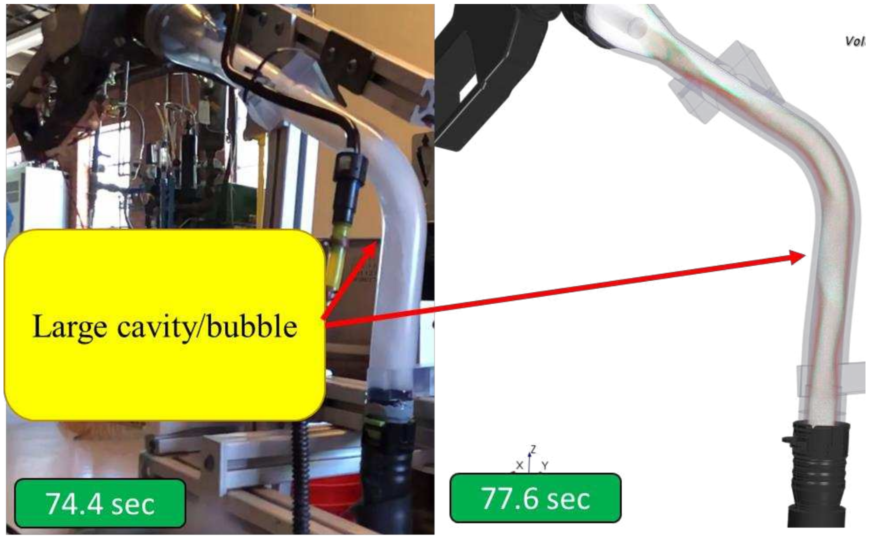

Figure 7.10 Click-off Phenomenon in 14GPM case (a)

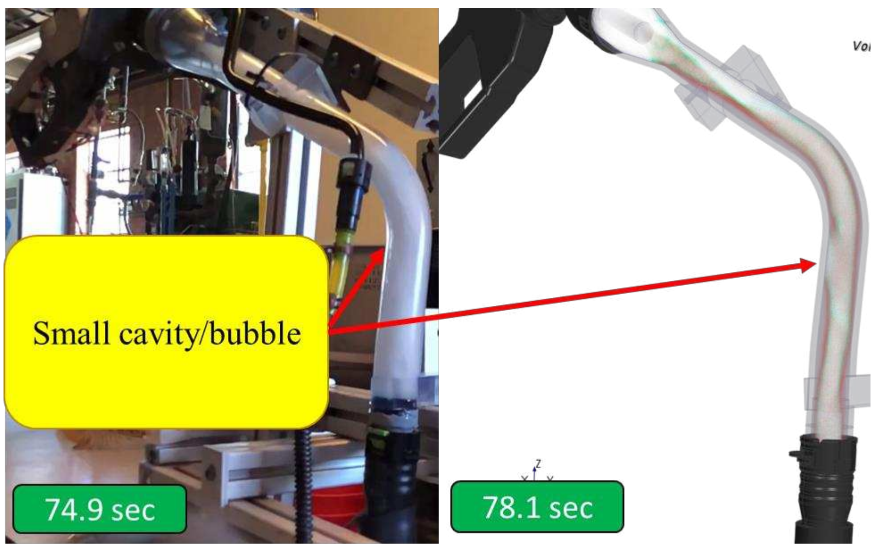

Figure 7.11 Click-off Phenomenon in 14GPM case (b)

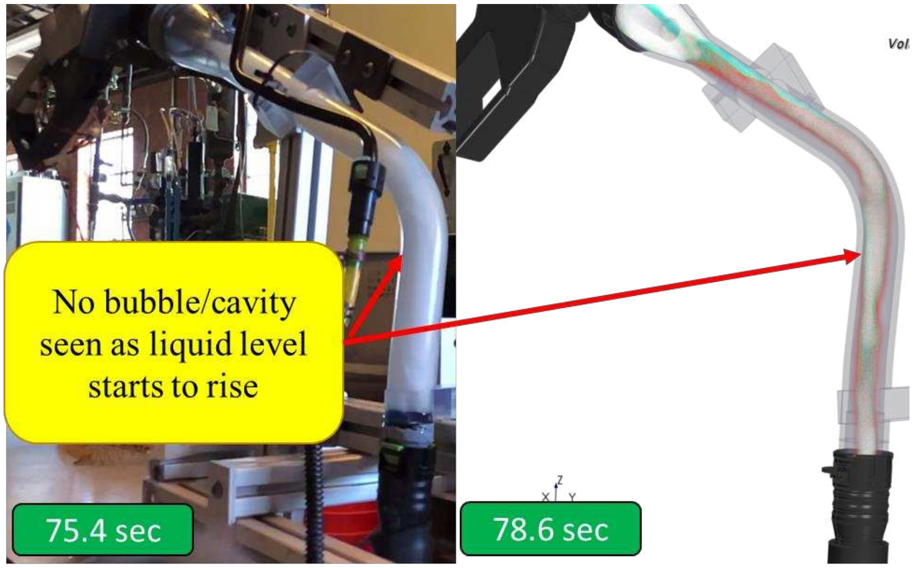

Figure 7.12 Click-off Phenomenon in 14GPM case (c)

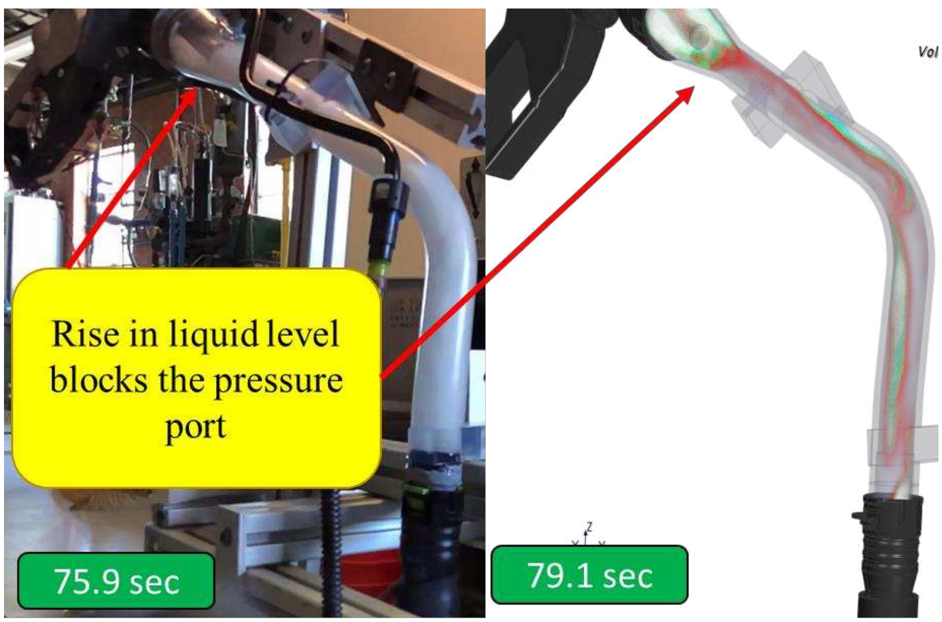

Figure 7.13 Click-off Phenomenon in 14GPM case (d)

8 Conclusions and Future Work

8.1 Part – I

The primary goal for Part - I of the study was to develop a computation fluid dynamic model capable of predicting the fluid dynamics within an open fillerpipe geometry which lead to click-off. Starting with carefully designed controlled experiments, the methodology related to the model geometry setup, boundary condition assignment (including the correct nozzle output), meshing and time stepping strategies were identified. Using the lessons learned from the staged model development, a CFD fillerpipe model was developed. The model when tested and compared to the performance of two different fillerpipes demonstrated the sensitivity to predict early click-off because of fluid recirculation near the nozzle outlet. Using pressure traces measured at multiple locations along the filler pipe and visualization data it was found that the predicted fluid dynamics trended correctly with the empirical data. The following highlights the major outcomes from Part - I of study:

1. Expertise with STAR-CCM+ has been gained related to modeling multiphase bubbly flows.
2. Using CATIA V5 in concert with STAR-CCM+, a procedure to setup the model geometry/alignment and mesh the internal volume was determined. This procedure will minimize user hours during the setup while still providing an accurate description of the fluid domain.
3. Two full-scale filler necks provided by Honda R&D were tested to evaluate if and at what angle/insertion depth of the fuel nozzle lead to early click-off. Results showed that one of the filler pipes demonstrated click-off at the angled nozzle conditions because of fluid recirculation near the inlet of the filler neck, while the other pipe properly functioned over all test conditions.

4. The simulation model is able predict early click-off which happens within the first few seconds of the refueling.

8.2 Part – II

Phase II of the study was focused on modeling the dynamics of the full refueling system. In order to ensure accurate description of the system in both the physical experiments and the simulations, the transient boundary conditions of the OWV and canister orifice were characterized. These tasks made up a significant portion of Phase II of the study. Experiments and simulations were performed to make sure all the boundary conditions used by the CFD model are correct. With the system fully described, refueling simulations and experiments were carried out with a low vapor pressure fuel while transiently tracking tank pressure, filler pipe flow, and the fuel dispense flow rate. Key outcomes of the Part – II of the study are listed below:

1. Real time flow rate data was added to filling tests via a new turbine flow meter. This allowed for greater understanding of pressure data. Inconsistencies in data were investigated using the flow data. The flow meter allowed identification of poorly performed experiments that needed to be repeated.
2. The boundary conditions of the Vapor Return Line (VRL) and canister line were characterized. This allowed accurate modeling of these components in CFD, improving accuracy of the simulation.
3. Repeatable experiments at 4, 10, and 14 GPM were performed. Data for tank pressure and fuel flow rate was gathered from each run.
4. Steady state tank pressures from CFD and experiments were compared. The results of either method trend the same with increasing flow rate. CFD pressure is higher than experiments by 100-150 Pa.

8.3 Future Work

In order to predict the evaporative emissions from the tank, evaporation physics (evaporation-condensation model) needs to be added to the current simulations. In addition, as a part of EPA testing procedure the prefilled and dispensed fuel has to be at different specified temperatures during refueling, therefore, the evaporation can also be affected by the heat transfer between the prefilled, the dispensed fuel, and the walls of the tank. Segregated Multiphase Temperature (SMT) model needs to be added to incorporate heat transfer. Stability criteria will also change as mass diffusion is going to be a prominent phenomenon. These additions greatly increase the complexity of the modeling and thus the computation time. Initial work has been carried out and tank pressures are higher in case of Indolene as compared to Stoddard fuel. A comparison of pressures inside the tank for Indolene versus Stoddard is shown in the Figure 8.1. Clearly, higher tank pressures result for Indolene as a result of evaporation indicating the need to include these physics in subsequent work. This work is currently underway to simulate the system with Indolene as fuel. Figure 8.2 shows a still image from these simulations.

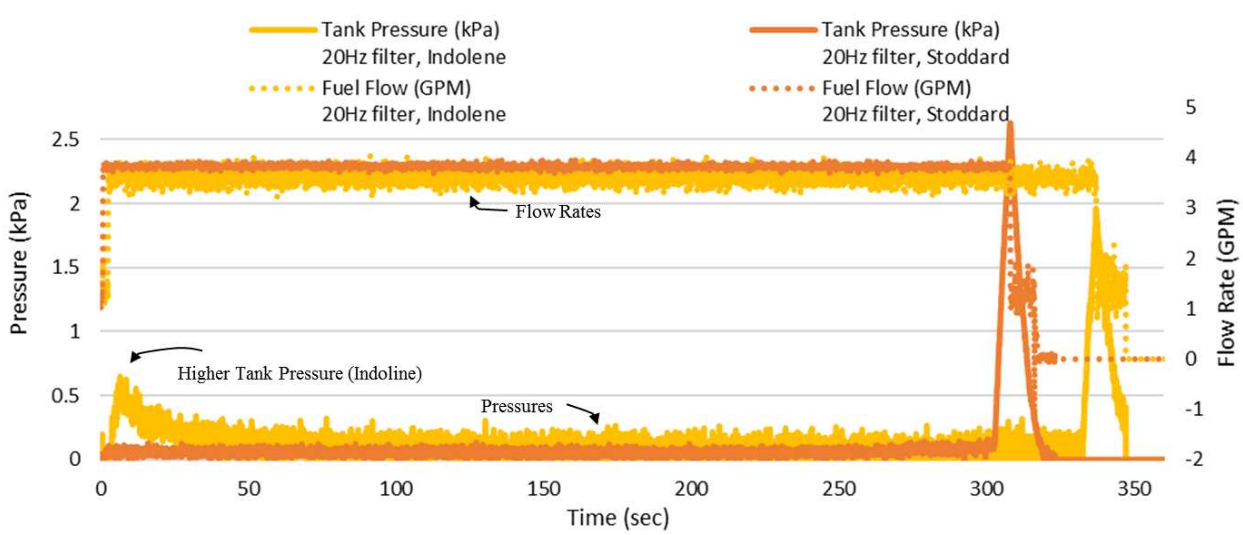

Figure 8.1 Tank pressure Stoddard vs. Indolene

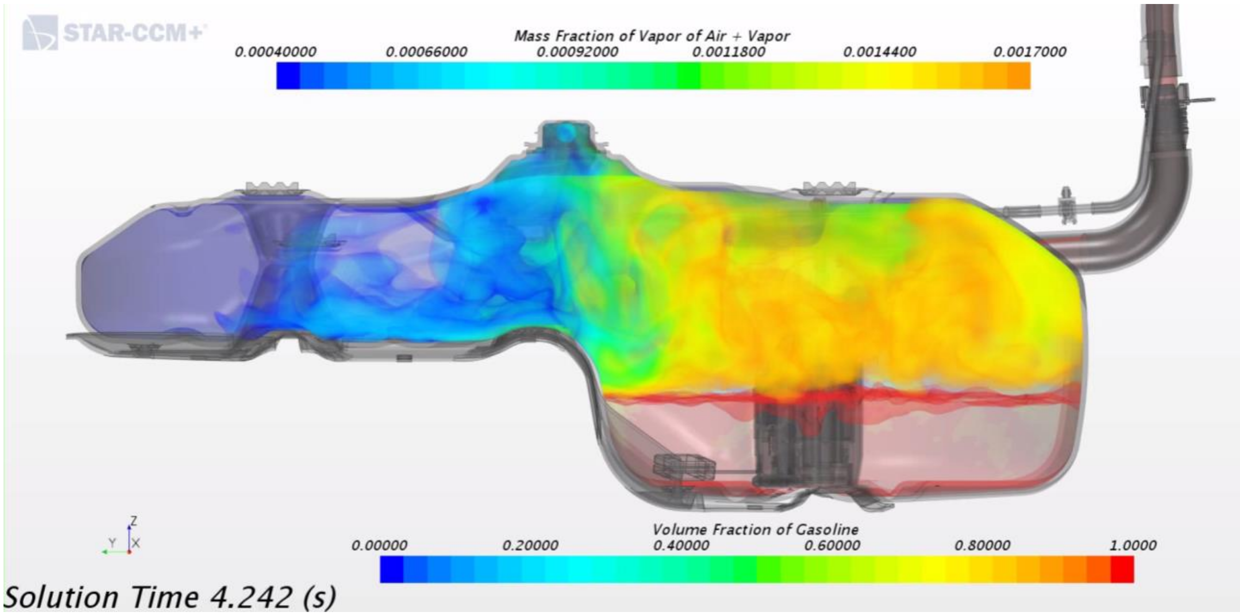

Figure 8.2 Fuel evaporation in the fuel tank

References

[1] T. Tiberi, “Stage II & ORVR and Associated Emissions of Gasoline Vapor,” *ARID Technol.*, pp. 1–18, 2012.

[2] EPA, “Fact Sheet: Final Rule Determining Widespread use of Onboard Refueling Vapor Recovery and Waiver of Stage Two Requirements.” 2012.

[3] EPA, “Transportation, Air Pollution, and Climate Change.” 2010.

[4] M. A. Abdelmajeed, M. H. Onsa, and A. A. Rabah, “Management of evaporation losses of gasoline’s storage tanks,” *Sudan Eng Soc J*, vol. 55, no. 52, pp. 39–45, 2009.

[5] S. Reddy, “Evaporative & Refueling Emission Control.” .

[6] F. Freda, “Onboard Refueling Vapor Recovery: Evaluation of the ORVR Program in the United States,” *ICCT*, 2011.

[7] W. J. Koehl, L. J. McCabe, and R. F. Becker, “Vehicle Refuelling Emission Control in the United States,” *Oil Gas—European Mag.*, vol. 1, pp. 36–40, 1987.

[8] S. ad Wiesche, “Simulation of automotive fuel tank filler pipe flows,” *Forsch. Im Ingenieurwesen*, pp. 139–149, 2004.

[9] M. Mastroianni, “Experimental investigation of automotive fuel tank filling.,” 2000.

[10] K. Johansson, “Numerical simulation of fuel filling with volume of fluid,” 2011.

[11] M. Gunnesby, *On Flow Predictions in Fuel Filler Pipe Design-Physical Testing vs Computational Fluid Dynamics*. 2015.

[12] R. Banerjee *et al.*, “CFD simulations of critical components in fuel filling systems,” SAE Technical Paper, 2002.

[13] A. Hassanvand, S. H. Hashemabadi, and M. Bayat, "Evaluation of gasoline evaporation during the tank splash loading by CFD techniques," *Int. Commun. Heat Mass Transf.*, vol. 37, no. 7, pp. 907–913, 2010.

[14] M. C. Lockhart, R. H. Thompson, and S. L. Baldus, "Methodology for evaluating fuel dispenser nozzle characteristics," SAE Technical Paper, 1997.

[15] S. G. Kandlikar, *Handbook of phase change: boiling and condensation*. CRC Press, 1999.

[16] A. Criscione, R. Röhrig, L. Opfer, I. Roisman, and S. Jakirlic, "Numerical investigation of impacting water drops in air cross-flow," in *ILASS—Europe 2011, 24th European Conference on Liquid Atomization and Spray Systems*, 2011.

[17] S. Gopalakrishnan and D. P. Schmidt, "A computational study of flashing flow in fuel injector nozzles," *SAE Int. J. Engines*, vol. 1, no. 1, pp. 160–170, 2009.

[18] S. Muzaferija, "Computation of free surface flows using interface-tracking and interface-capturing methods," *Nonlinear Water-Wave Interact. Comput. Mech. Southampt.*, 1998.

[19] L. D. Landau and E. M. Lifshitz, *Course of theoretical physics*. Elsevier, 2013.

[20] S. S. Sazhin, "Advanced models of fuel droplet heating and evaporation," *Prog. Energy Combust. Sci.*, vol. 32, no. 2, pp. 162–214, 2006.

[21] K. Neroorkar, S. Gopalakrishnan, R. O. Grover Jr, and D. P. Schmidt, "Simulation of flash boiling in pressure swirl injectors," *At. Sprays*, vol. 21, no. 2, 2011.

[22] K. Yokoi, D. Vadillo, J. Hinch, and I. Hutchings, "Numerical studies of the influence of the dynamic contact angle on a droplet impacting on a dry surface," *Phys. Fluids*, vol. 21, no. 7, p. 072102, 2009.

[23] Siemens, "STAR CCM+ User Guide." .

[24] R. Banerjee, K. M. Isaac, L. Oliver, and W. Breig, “A numerical study of automotive gas tank filler pipe two phase flow,” SAE Technical Paper, 2001.

[25] R. Banerjee, C. Burke, and D. Gepper, “Experimental and numerical study of gasoline refueling nozzle spray pattern,” SAE Technical Paper, 2007.

[26] J. W. Stansbury and M. J. Idacavage, “3D printing with polymers: Challenges among expanding options and opportunities,” *Dent. Mater.*, vol. 32, no. 1, pp. 54–64, 2016.

[27] D. Wu, S. Li, and P. Wu, “CFD simulation of flow-pressure characteristics of a pressure control valve for automotive fuel supply system,” *Energy Convers. Manag.*, vol. 101, pp. 658–665, 2015.

[28] Y. Hou, J. Chen, L. Zhu, D. Sun, J. Li, and P. Jie, “Numerical simulation of gasoline evaporation in refueling process,” *Adv. Mech. Eng.*, vol. 9, no. 8, p. 1687814017714978, 2017.

[29] G. A. Lavoie, Y. A. Imai, and P. J. Johnson, “A fuel vapor model (FVSMOD) for evaporative emissions system design and analysis,” SAE Technical Paper, 1998.

[30] H. C. Hartsell Jr, E. A. Payne, P. D. Miller, and M. B. Tucker, *Onboard vapor recovery detection*. Google Patents, 1998.

[31] J. G. Collier and J. R. Thome, *Convective boiling and condensation*. Clarendon Press, 1994.

[32] L. G. Dodge and J. A. Schwalb, “Fuel spray evolution: comparison of experiment and CFD simulation of nonevaporating spray,” *J. Eng. Gas Turbines Power*, vol. 111, no. 1, pp. 15–23, 1989.

[33] G. X. Wu, Q. W. Ma, and R. E. Taylor, “Numerical simulation of sloshing waves in a 3D tank based on a finite element method,” *Appl. Ocean Res.*, vol. 20, no. 6, pp. 337–355, 1998.